The zonal patterns in late Quaternary South American Monsoon precipitation

Tyler Kukla[1], Matthew Winnick[2], Marysa Laguë[3], and Zhengyu Xia[4]

[1]Colorado State University
[2]University of Massachusetts Amherst
[3]James S. McDonnell Foundation
[4]Northeast Normal University

December 31, 2022

Abstract

Speleothem oxygen isotope records (δ18O) of tropical South American rainfall in the late Quaternary show a zonal "South American Precipitation Dipole" (SAPD). The dipole is characterized by opposing east-west precipitation anomalies compared to the present—wetter in the east and drier in the west at the mid-Holocene (7 ka), and drier in the east and wetter in the west at the Last Glacial Maximum (LGM; 21 ka). However, the SAPD remains enigmatic because it is expressed differently in western versus eastern δ18O records and isotope-enabled climate model simulations usually misrepresent the magnitude and/or spatial pattern of δ18O change. Here, we address the SAPD enigma in two parts. First, we re-interpret the δ18O data to account for upwind rainout effects that are known to be pervasive in tropical South America, but are not always considered in Quaternary paleoclimate studies. Our revised interpretation reconciles the δ18O data with cave infiltration and other proxy records, and indicates that the centroid of tropical South American rainfall has migrated zonally over time. Second, using an energy balance model of tropical atmospheric circulation, we hypothesize that zonal migration of the precipitation centroid can be explained by regional energy budget shifts, such as changing Saharan albedo associated with the African Humid Period, that have not been modeled in previous SAPD studies. This hypothesis of a migrating precipitation centroid presents a new framework for interpreting δ18O records from tropical South America and may help explain the zonal rainfall anomalies that predate the late Quaternary.

Supporting Information for "The zonal patterns in late Quaternary tropical South American precipitation"

T. Kukla[1,2], M. J. Winnick[3], M. M. Laguë[4,5], Z. Xia[3,6]

[1]Department of Geosciences, Colorado State University, Fort Collins, CO, USA

[2]Department of Geological Sciences, Stanford University, Stanford, CA, USA

[3]Department of Geosciences, University of Massachusetts Amherst, Amherst, MA, USA

[4]University of Saskatchewan Coldwater Lab, Canmore, Alberta, Canada

[5]Department of Atmospheric Sciences, University of Utah, Salt Lake City, UT, USA

[6]Key laboratory of Geogrpahical Processes and Ecological Security in Changbai Mountains, Ministry of Education, School of Geographical Sciences, Northeast Normal University, Changchun, China

Contents of this file

Text S1: Quantifying moisture recycling connectivity between eastern, central, and western records

The first goal of the paper is to interpret past rainfall patterns from the spatial isotope gradient (negative $\Delta\delta^{18}O$ indicates decreasing $\delta^{18}O$ moving inland), rather than the individual $\delta^{18}O$ records themselves. Critically, this interpretive framework only holds if the three speleothem sites are isotopically connected, meaning that changes in $\delta^{18}O$ that occur at one site are propagated downwind to the other sites (Salati et al., 1979; Hu et al., 2008;

Winnick et al., 2014; Kukla et al., 2019). However, the extent to which an upwind $\delta^{18}O$ signal is transferred downwind between sites is difficult to constrain with reanalysis data. Instead, we quantify the moisture recycling connectivity, or how much moisture reaches two sites along a transect. Moisture that is recycled across both sites of a transect will necessarily carry the isotopic signature of its upwind rainout and evaporation.

To validate our use of the isotope gradient approach, we quantify the moisture recycling connectivity of the three sites using the two-atmospheric-layer water accounting model (WAM-2layers) of van der Ent, Wang-Erlandsson, Keys, and Savenije (2014) and the precipitation back-tracking scheme of Keys et al. (2012) (van der Ent & Savenije, 2013; van der Ent, 2016). We run the model for all three speleothem sites where each site is represented by a 3x3 grid of 1.5 degree cells, following Cluett, Thomas, Evans, and Keys (2021). The WAM-2layers forward and backward tracking schemes output evaporationsheds and precipitationsheds, respectively, where a site's evaporation-shed is the region where local evaporation re-precipitates and its precipitationshed is the region where its precipitation is sourced via evaporation. We can approximate the degree of moisture recycling connectivity by analyzing the precipitation- and evaporationshed threshold, or the probabilistic region encompassing some percentage of total rainfall, wherein two sites exist within the same "-shed" (Keys et al., 2012). A lower threshold indicates a stronger recycling connection. For example, at a given site, every grid cell contributes at least an infinitesimally small amount of vapor to local rainfall, so the 100% precipitationshed threshold encompasses the entire globe. Keys et al. (2012) set a threshold of 70% to encompass meaningful regional dynamics and moisture recycling connections for precipitationsheds. We find that the eastern and central sites are connected with a precipitationshed threshold of 36% (evaporationshed threshold of 63%), and the central and western sites with a precipitation-shed threshold of 48% (evaporation-shed threshold of 32%) (see main text).

This hydrologic connection is rather robust across the annual cycle, with upwind sites providing moisture to downwind sites throughout the wet season (Fig. S2 and year-round (Fig. S2.

These precipitation-shed thresholds likely underestimate the true moisture recycling connectivity. Precipitation-sheds only include moisture that has been recycled once (*i.e.* a single instance of evaporation and re-precipitation). However, it is likely that a substantial fraction of moisture between these sites (especially from central to western) is recycled more than once (Zemp et al., 2014), meaning not all of the moisture reaching each site is accounted for in our analysis. Additionally, the isotopic signal of upwind rainout (*i.e.* the decrease in $\delta^{18}O$ from a moisture-depleted airmass) will propagate downwind, even if the upwind precipitation itself does not. Thus, the isotopic connectivity is underestimated by the moisture recycling connectivity. Based on this result, we find that the eastern-to-central and central-to-western isotope gradients are sufficiently hydrologically connected to interpret their $\Delta\delta^{18}O$ trends. Because such a large fraction of western (central) rainout is sourced from the central (eastern) site, oxygen isotope signals at the upwind site are likely to propagate downwind in the climatological mean. This analysis indicates relative changes in $\Delta\delta^{18}O$ likely relate to air mass rainout among all sites, but we focus exclusively on the central-to-western gradient to *quantify* rainfall trends from $\Delta\delta^{18}O$ data because the trajectory aligns more closely with prevailing monsoon winds.

Text S2: Reactive transport model assumptions and limitations

The general assumptions and limitations of the RTM are described in section 2.4 of Kukla et al. (2019). Two of these limitations are relevant for our analysis. These are 1) the assumption of isotopes in precipitation reflecting mean annual conditions and 2) the limitation of the model to "single storm track" systems.

First, the implementation of the Budyko framework requires the assumption that fluxes of P, ET, and E_0 reflect climatological mean values. The limits to ET in the Budyko solution space do not apply on seasonal or even annual timescales where water storage cannot be assumed constant. This means that our model cannot meaningfully evaluate possible seasonal biases that may weaken the relationship between $\delta^{18}O$ and long-term mean conditions if changes in water storage are significant. However, we do not expect these biases to significantly influence our analysis for two reasons. First, these biases often affect single-site $\delta^{18}O$ records on a regional scale. If each study site is equally influenced by the same regional bias, this will not affect our $\Delta\delta^{18}O$ data. Second, the isotope gradient ($\Delta\delta^{18}O$) in the Amazon varies seasonally in the same direction as expected with changes in the seasonal water balance (shallower in the dry season, steeper in the wet season) (Fig. S4), suggesting the isotope gradient is a robust tracer of the mean annual water balance (as it tracks the water balance year-round).

A second limitation to the application of our model is based on the assumption of a single storm track. The RTM cannot simulate mixing between different storm trajectories and instead assumes that precipitation is delivered across a 1-dimensional domain from a single source. Presently, a robust definition for a "single storm track" remains elusive, but we note a few conditions that lend confidence to the RTM application (following Kukla et al. (2019)). First, dramatic seasonal or climatological variability in the direction of moisture transport is incompatible with the RTM. Despite the monsoon climate of the Amazon Basin, seasonal changes in wind direction do not appear to strongly bias the $\Delta\delta^{18}O$, as evidenced in the application to modern data in Kukla et al. (2019) and the good agreement between simulated mean annual precipitation in our Pre-Industrial (LH) Monte Carlo simulations. This could be due to similar transport distances across the continent between seasons (despite its "monsoon" designation, wind directions in South America show less seasonal variability than most other monsoonal regions), possible incorporation of wet season rain in dry season moisture, or that even seasonal changes in monsoonal wind directions are not great enough to violate the single storm track assumption.

Text S3: Isotopic effects of convection

A number of previous studies have demonstrated that both micro- and macro-physical processes associated with deep convection may result in a number of distinct isotopic effects on resulting precipitation. Microphysical processes are unlikely to be the main driver of the "amount effect" as it is well-documented that the correlation between $\delta^{18}O$ and precipitation amount breaks down at small scales (Kurita et al., 2009; Moerman et al., 2013; Moore et al., 2014; Aggarwal et al., 2016; Conroy et al., 2016; Konecky et al., 2019). In its original formulation, the RTM used here does not explicitly simulate convective processes like vertical downdrafts and dry air entrainment, altitude-dependent changes in vertical velocity, and precipitation efficiency. In this section, we describe the possible isotopic effects associated with convective processes, the baseline representation of macro-scale processes such precipitation efficiency, re-evaporation, and stratiform versus convective rain in our model framework, and a model sensitivity analysis to post-condensation evaporation.

Recycling of water vapor in the convective cloud and stratiform vs. convective rain

Previous studies have shown that two primary sources contribute to moisture within convective clouds 1) an oceanic source and 2) a local, sub-cloud evaporation source. These two sources are explicitly represented in our mass balance equations, as the moisture available for precipitation is the sum of transported and local surface-evapotranspired vapor. Indeed, the balance between these two sources is widely cited as the primary driver of the tropical "amount effect"—the negative correlation between $\delta^{18}O$ and precipitation amount (Rozanski et al., 1993; Lee & Fung, 2008; Lee et al., 2009; Moore et al., 2014; Bailey et al., 2018). Because transport balances precipitation minus evapotranspiration, the ratio of transported to evapotranspired moisture (γ) can be represented by:

$$\gamma \equiv -\frac{P-E}{E} \quad (1)$$

Where P is precipitation and E is evaporation. The "amount effect" emerges because in tropical oceans and most tropical land masses (including Amazonia), E is limited by potential evapotranspiration or the energy available for evaporation, such that P is the primary driver of changes in γ (potential evaporation does not vary much in the tropics). Thus the constraint of potential evapotranspiration on evapotranspiration provides a robust representation of the "amount effect" as the balance of P and E in our model.

We note that an alternative hypothesis for the tropical "amount effect" argues that it is driven by the proportion of convective versus stratiform precipitation (Kurita, 2013; Aggarwal et al., 2016; Konecky et al., 2019). However, large scale circulation that generates stratiform precipitation balances P-minus-E (numerator of equation 1), whereas convection mostly sources local evaporation (denominator of equation 1) (Moore et al., 2014). Thus, the balance of convective and stratiform precipitation is necessarily related to γ (Moore et al., 2014) which is represented in our model.

Sensitivity analysis of post-condensation re-evaporation

In atmospheric circulation models, re-evaporation determines how much condensed vapor reaches the ground as precipitation (i.e. "precipitation efficiency"). Precipitation efficiency parameterizations exert significant influence over modeled climate and are often used as tuning parameters for global hydroclimate as in the MERRA2 reanalysis product (Bacmeister et al., 2006; Molod et al., 2015).

However, the extent of isotopic effects of post-condensation evaporation is not well characterized. Theoretically, the extent of fractionation during re-evaporation depends primarily on whether all raindrops partially re-evaporate to a similar extent (large fractionation signal) or if re-evaporation is skewed towards the full evaporation of smaller droplets with minimal partial evaporation of larger droplets (minimal fractionation signal). Drop sizes and their role in re-evaporation are usually parameterized and are not well-constrained (e.g. Lee and Fung (2008)). Thus, while MERRA2 reanalysis estimates 50-60% of tropical condensed moisture evaporates before reaching land (Konecky et al., 2019) the magnitude of isotopic effects are not well characterized.

Observational studies have aimed to quantify the effect of re-evaporation on vapor and precipitation isotopes (Worden et al., 2007; Konecky et al., 2019). Direct measurements of this effect are extremely difficult, and existing studies rely on correlations between isotopes and climate conditions. For example, Worden et al. (2007) use Tropospheric Emission Spectrometer (TES) data to argue low δD at high specific humidity in the tropics is due to re-evaporation. However, whether the TES can resolve re-evaporation signals in convection remains an open question (Duan et al., 2018). Using direct precipitation measurements, Konecky et al. (2019) notes a correlation between $\delta^{18}O$ of precipitation and MERRA2 estimates of rainfall re-evaporation, though confounding factors such as the stratiform fraction (or P/E balance) may influence this relationship as they are used to calculate re-evaporation in MERRA2 (Bacmeister et al., 2006; Molod et al., 2015). Thus, while observational studies indicate correlations between local rainfall $\delta^{18}O$ and metrics of re-evaporation, it remains unclear how sensitive $\delta^{18}O$ is to re-evaporation alone. Additionally, cloud-resolving model simulations suggest that re-evaporation has a minimal effect on the isotopic "amount effect" (Moore et al., 2014).

Isotope-enabled models calibrated to global precipitation $\delta^{18}O$ also indicate minimal isotopic effects of post-condensation evaporation. Dee, Noone, Buenning, Emile-Geay, and Zhou (2015) calibrate re-evaporation to global $\delta^{18}O$ data using an isotope-enabled, simple-physics atmospheric GCM, "SPEEDY-IER". Their approach may help disentangle how much of the total re-evaporation flux affects isotopes (via partial drop evaporation). They find that the spatial distribution of isotopes is strongly influenced by the re-evaporation parameterization. Using the re-evaporation formulation of Sundqvist (1988), re-evaporation (Eprec) in SPEEDY-IER is:

$$E_{prec} = K_E(1 - h)\sqrt{P} \tag{2}$$

Where E_{prec} depends on humidity (h), precipitation (P) and a coefficient K_E. E_{prec} increases with lower humidity and with more precipitation. However, isotope fractionation is proportional to the fraction of evaporated moisture (E_{prec}/P) and the re-evaporation fraction decreases as precipitation (P) increases. Dee et al. (2015) find that K_E of ∼0.03 provides the best fit to global $\delta^{18}O$ (where fluxes have units of g m-2 s-1). With this parameterization, the re-evaporation fraction is far lower than MERRA2 suggests for the tropics, suggesting that most re-evaporation involves total droplet evaporation and does not affect precipitation $\delta^{18}O$.

To test the sensitivity of our results to post-condensation re-evaporation effects, we modify the isotope module of our RTM to include the re-evaporation fraction and force it with three scenarios following the parameterization of Dee et al. (2015) (Fig. S6). The first is a control scenario where we initialize the RTM with Amazon climatology and no re-evaporation flux. In the second scenario we assume the unlikely case that re-evaporation affects the $\delta^{18}O$ of all raindrops equally, regardless of size. We assume tropical E_{prec}/P is 0.55 (from the range of Konecky et al. (2019)). This is the largest effect re-evaporation could have on $\delta^{18}O$ but is unlikely because it does not account for total re-evaporation of the smallest droplets (Lee & Fung, 2008) and is inconsistent with isotope-enabled climate model calibrations. In the third scenario we assume the isotopic effect of re-evaporation follows the parameterization of (Dee et al., 2015). Adopting the conservative (highest E_{prec}/P) estimates of P=2.4m/yr and h=0.5 we find E_{prec}=0.05 in the Amazon (equation 1). Higher values of h and P, both expected on the timescale of a storm event when E_{prec} matters for precipitation, lead to lower E_{prec}/P and therefore an even smaller effect on precipitation $\delta^{18}O$.

We use the RTM to interpret the spatial isotope gradient rather than absolute $\delta^{18}O$ values (Fig. S6), so we discuss the effect of re-evaporation on RTM $\Delta\delta^{18}O$ here. When all re-evaporation leads to isotope fractionation, the modeled isotope gradient is -2.8‰/1,000km, steeper than the steepest isotope gradient documented in the last ~40 kyr (the extent of the proxy data; -2.5‰/1,000km). By contrast, when the RTM is run with E_{prec}/P values derived from the optimization of Dee et al. (2015), re-evaporation has a negligible effect on $\Delta\delta^{18}O$, leading to a decrease of only 0.08‰/1,000km which is well within the uncertainty from the proxy data (+/- 0.3‰/1,000 km) (Fig. S6).

Taken together, we maintain that it is appropriate to omit a re-evaporation scheme in our analysis in the main text for three reasons: 1) There is no strong observational evidence supporting a large-scale link between isotopes and re-evaporation; 2) the RTM is successful at simulating modern precipitation $\delta^{18}O$ when forced with modern climatology, suggesting it already represents the important physical processes; and 3) The globally-calibrated parameterization of Dee et al. (2015) suggests tropical precipitation $\delta^{18}O$ is insensitive to the incorporation of re-evaporation into our model. The Dee et al. (2015) parameterization optimizes the fit to modern precipitation $\delta^{18}O$ and, therefore, serves as an indication of how re-evaporation affects the isotope balance. The discrepancy between the large re-evaporation rates required to simulate tropical hydroclimate (e.g. (Bacmeister et al., 2006; Molod et al., 2015; Konecky et al., 2019)) and the small re-evaporation rates required to simulate its isotopes (Dee et al., 2015); Fig. S6) suggests that re-evaporation mostly occurs by the total evaporation of smaller raindrops that have no effect on precipitation $\delta^{18}O$.

Text S4: Comparing the three speleothem $\delta^{18}O$ signals to global records

To contextualize our estimated change in Amazon rainfall from the LGM to the mid-Holocene and begin hypothesizing the underlying dynamic driver, we compare the magnitude of $\delta^{18}O$ change at each site (eastern, central, and western) to similar global records. We compile all records from the SISALv2 database that span more than 10000 years (Atsawawaranunt et al., 2018; Comas-Bru et al., 2019, 2020), the approximate duration from the peak-to-trough of a precession cycle. We filter out records that are exceptionally long ($>$ 100kyr) because the range of $\delta^{18}O$ increases with the duration of the record above this threshold, but is mostly independent of the record duration below. Finally, we only analyze records with an absolute latitude less than 40 degrees to isolate tropical and sub-tropical climates. To account for variations from site to site in the high-frequency "noise" of the data, all records are smoothed with a 1000 yr moving average and re-sampled to the same resolution (including the tropical South America sites). We calculate the standard deviation (not shown) and range of each record and compare to the three records of interest.

Text S5: Toy model of phase of precipitation seasonality and $\Delta\delta^{18}O$

The goal of this section is to test whether the phase of precipitation seasonality can impact $\Delta\delta^{18}O$ independent of net rainout. We simulate $\Delta\delta^{18}O$ between two sites throughout the year, varying the difference in the phase of precipitation seasonality and the amplitude of seasonal $\delta^{18}O$ (thus, $\Delta\delta^{18}O$). We first prescribe some seasonal cycle of precipitation upwind of site 1 (the eastern, or upwind site). Since we only care about differences in the phase of precipitation seasonality between sites (and, being the tropics, we ignore temperature seasonality), we hold the upwind seasonal cycle of precipitation constant. Upwind rainout at site 1 set as:

$$P_{s1,upwind} = A \times cos\,(2\pi \times t) + A \tag{3}$$

where A is the amplitude, t is time (fraction of year from zero to one), and the amplitude is added to the end to avoid negative precipitation rates. $P_{s1,upwind}$ represents the integrated upwind rainout that occurs at the upwind site. We then calculate $P_{s2,upwind}$, the integrated rainout between sites (upwind of site 1, downwind of site 2), using the same sine curve as $P_{s1,upwind}$ with some phase shift, ϕ:

$$P_{s2,upwind} = A \times cos\,(2\pi \times t + \phi) + A. \tag{4}$$

The oxygen isotope composition of rainfall at the upwind site (site 1) is calculated assuming that source moisture $\delta^{18}O$ equals zero and $\delta^{18}O$ is anti-correlated with upwind rainfall with some slope, m:

$$\delta^{18}O_{s1} = 0 - \left(\frac{P_{s1,upwind}}{m}\right). \tag{5}$$

Downwind $\delta^{18}O$ (site 2) is calculated the same way, just substituting $\delta^{18}O_{s1}$ for zero:

$$\delta^{18}O_{s2} = \delta^{18}O_{s1} - \left(\frac{P_{s2,upwind}}{m}\right). \tag{6}$$

Finally, we take the $\delta^{18}O$ difference between sites to get $\Delta\delta^{18}O$, then calculate the climatological $\Delta\delta^{18}O$ by taking the precipitation-weighted annual mean. We repeat these calculations for changes in the phase, ϕ, and relative $\delta^{18}O$ seasonal amplitude, captured by the slope term m. The results are shown in Figs. S11 and S12.

The model results show that changes in the relative phase of precipitation from one site to the next do not invalidate $\Delta\delta^{18}O$ as a proxy for net rainout. The error introduced by phase differences between sites is non-zero, but it is negligible—consistently less than 1% of the seasonal amplitude of $\Delta\delta^{18}O$. Given a $\Delta\delta^{18}O$ seasonal amplitude of $\sim$2‰/1000km from the eastern-to-central sites today, differences in the timing of eastern and central peak precipitation should impact $\Delta\delta^{18}O$ by less than 0.02‰/1000 km.

Text S6: Testing seasonal climate anomalies with results of Liu & Battisti, 2015

Liu & Battisti show that, in their simulations, the decrease in $\delta^{18}O$ in northeastern Brazil as austral summer insolation decreases is driven by more DJFMA precipitation and lower wet-season $\delta^{18}O$. Here, we analyze how their seasonal precipitation and $\delta^{18}O$ anomalies can be reconciled with the observed amplitude of northeastern Brazil $\delta^{18}O$ change of ∼5-7‰. We digitize their monthly northeastern Brazil results (Fig. 7 of Liu and Battisti (2015)) using Engauge Digitizer (Fig. S8A), and we test three sets of simulated anomalies (Fig. S8B). First, we test whether increasing wet season (DJFMA) and decreasing dry season (JJA) rainfall can cause a 5-7‰ $\delta^{18}O$ shift, holding the seasonal cycle of $\delta^{18}O$ constant. Because JJA rainfall is at zero for their high- and low-insol experiments, we use the modern observed precipitation seasonality for the control case. We find no reasonable change in precipitation seasonality that is capable of explaining the amplitude of eastern $\delta^{18}O$ change.

Next, we test the role of JJA and DJFMA precipitation $\delta^{18}O$ anomalies. Due to low JJA rainfall (even using modern observations as the initial, control case) JJA $\delta^{18}O$ has a negligible effect on precipitation-weighted $\delta^{18}O$, whereas DJFMA $\delta^{18}O$ has a much larger effect. Still, DJFMA $\delta^{18}O$ would have to decrease by 5-7‰ relative to the high_insol case in order to match the eastern domain $\delta^{18}O$ record (about a 4x larger change in $\delta^{18}O$ than found in the simulations of Liu and Battisti (2015). This result holds even in our third experiment, where we allow DJFMA precipitation amounts to increase. We conclude that, given the simulated seasonal cycle of precipitation or $\delta^{18}O$ in Liu and Battisti (2015), a much larger decrease in wet-season $\delta^{18}O$ is required to explain the eastern speleothem $\delta^{18}O$ data—consistent with a zonal shift in the precipitation centroid.

Figures S1-S12

References

Aggarwal, P. K., Romatschke, U., Araguas-Araguas, L., Belachew, D., Longstaffe, F. J., Berg, P., ... Funk, A. (2016, August). Proportions of convective and stratiform precipitation revealed in water isotope ratios. *Nature Geoscience*, *9*(8), 624–629. doi: 10.1038/ngeo2739

Atsawawaranunt, K., Comas-Bru, L., Mozhdehi, S. A., Deininger, M., Harrison, S. P., Baker, A., ... Scroxton, N. (2018). The SISAL database: A global resource to document oxygen and carbon isotope records from speleothems. *Earth System Science Data*, *10*, 1687–1713.

Bacmeister, J. T., Suarez, M. J., & Robertson, F. R. (2006, December). Rain Reevaporation, Boundary Layer–Convection Interactions, and Pacific Rainfall Patterns in an AGCM. *Journal of the Atmospheric Sciences*, *63*(12), 3383–3403. doi: 10.1175/JAS3791.1

Bailey, A., Posmentier, E., & Feng, X. (2018, July). Patterns of evaporation and precipitation drive global isotopic changes in atmospheric moisture. *Geophysical Research Letters*, *45*, 7093–7101. doi: 10.1029/2018GL078254

Chamberlain, C. P., Winnick, M. J., Mix, H. T., Chamberlain, S. D., & Maher, K. (2014). The impact of neogene grassland expansion and aridification on the isotopic composition of continental precipitation. *Global Biogeochemical Cycles*, *28*(9), 992–1004. doi: 10.1002/2014GB004822

Cluett, A. A., Thomas, E. K., Evans, S. M., & Keys, P. W. (2021, June). Seasonal Variations in Moisture Origin Explain Spatial Contrast in Precipitation Isotope Seasonality on Coastal Western Greenland. *Journal of Geophysical Research: Atmospheres*, *126*(11). doi: 10.1029/2020JD033543

Comas-Bru, L., Harrison, S. P., Werner, M., Rehfeld, K., Scroxton, N., Veiga-Pires, C., & SISAL working group members. (2019, August). Evaluating model outputs using integrated global speleothem records of climate change since the last glacial. *Climate of the Past*, *15*(4), 1557–1579. doi: 10.5194/cp-15-1557-2019

Comas-Bru, L., Rehfeld, K., Roesch, C., Amirnezhad-Mozhdehi, S., Harrison, S. P., Atsawawaranunt, K., ... SISAL Working Group members (2020, October). SISALv2: A comprehensive speleothem isotope database with multiple age–depth models. *Earth System Science Data*, *12*(4), 2579–2606. doi: 10.5194/essd-12-2579-2020

Conroy, J. L., Noone, D., Cobb, K. M., Moerman, J. W., & Konecky, B. L. (2016, April). Paired stable isotopologues in precipitation and vapor: A case study of the amount effect within western tropical Pacific storms: Isotopes in Western Pacific Storms. *Journal of Geophysical Research: Atmospheres*, *121*(7), 3290–3303. doi: 10.1002/2015JD023844

Dee, S., Noone, D., Buenning, N., Emile-Geay, J., & Zhou, Y. (2015, January). SPEEDY-IER: A fast atmospheric GCM with water isotope physics. *Journal of Geophysical Research: Atmospheres*, *120*(1), 73–91. doi: 10.1002/2014JD022194

Duan, S. Q., Wright, J. S., & Romps, D. M. (2018, February). On the Utility (or Futility) of Using Stable Water Isotopes to Constrain the Bulk Properties of Tropical Convection. *Journal of Advances in Modeling Earth Systems*, *10*(2), 516–529. doi: 10.1002/2017MS001074

Hu, C., Henderson, G. M., Huang, J., Xie, S., Sun, Y., & Johnson, K. R. (2008, February). Quantification of Holocene Asian monsoon rainfall from spatially separated cave records. *Earth and Planetary Science Letters*, *266*(3-4), 221–232. doi: 10.1016/j.epsl.2007.10.015

Keys, P. W., van der Ent, R. J., Gordon, L. J., Hoff, H., Nikoli, R., & Savenije, H. H. G. (2012, February). Analyzing precipitationsheds to understand the vulnerability of rainfall dependent regions. *Biogeosciences*, *9*(2), 733–746. doi: 10.5194/bg-9-733-2012

Konecky, B. L., Noone, D. C., & Cobb, K. M. (2019, February). The Influence of Competing Hydroclimate Processes on Stable Isotope Ratios in Tropical Rainfall. *Geophysical Research Letters*, *46*(3), 1622–1633. doi: 10.1029/2018GL080188

Kukla, T., Winnick, M. J., Maher, K., Ibarra, D. E., & Chamberlain, C. P. (2019, January). The Sensitivity of Terrestrial δ [18] O Gradients to Hydroclimate Evolution. *Journal of Geophysical Research: Atmospheres*, *124*, 563–582. doi: 10.1029/2018JD029571

Kurita, N. (2013, September). Water isotopic variability in response to mesoscale convective system over the tropical ocean: ISOTOPES IN OCEANIC MOISTURE. *Journal of Geophysical Research: Atmospheres*, *118*(18), 10,376–10,390. doi: 10.1002/jgrd.50754

Kurita, N., Ichiyanagi, K., Matsumoto, J., Yamanaka, M. D., & Ohata, T. (2009, September). The relationship between the isotopic content of precipitation and the precipitation amount in tropical regions. *Journal of Geochemical Exploration*, *102*(3), 113–122. doi: 10.1016/j.gexplo.2009.03.002

Lee, J.-E., & Fung, I. (2008). "Amount effect" of water isotopes and quantitative analysis of post-condensation processes. *Hydrological Processes*, *2274*(November 2008), 2267–2274. doi: 10.1002/hyp

Lee, J.-E., Johnson, K., & Fung, I. (2009). Precipitation over South America during the Last Glacial Maximum: An analysis of the "amount effect" with a water isotope-enabled general circulation model. *Geophysical Research Letters*, *36*(19), L19701.

doi: 10.1029/2009GL039265

Liu, X., & Battisti, D. S. (2015, June). The Influence of Orbital Forcing of Tropical Insolation on the Climate and Isotopic Composition of Precipitation in South America. *Journal of Climate*, *28*(12), 4841–4862. doi: 10.1175/JCLI-D-14-00639.1

Moerman, J. W., Cobb, K. M., Adkins, J. F., Sodemann, H., Clark, B., & Tuen, A. A. (2013, May). Diurnal to interannual rainfall δ18O variations in northern Borneo driven by regional hydrology. *Earth and Planetary Science Letters*, *369–370*, 108–119. doi: 10.1016/j.epsl.2013.03.014

Molod, A., Takacs, L., Suarez, M., & Bacmeister, J. (2015, May). Development of the GEOS-5 atmospheric general circulation model: Evolution from MERRA to MERRA2. *Geoscientific Model Development*, *8*(5), 1339–1356. doi: 10.5194/gmd-8-1339-2015

Moore, M., Kuang, Z., & Blossey, P. N. (2014). A moisture budget perspective of the amount effect. *Geophysical Research Letters*, *41*(4), 1329–1335. doi: 10.1002/2013GL058302

Rozanski, K., Araguás-Araguás, L., & Gonfiantini, R. (1993). Isotopic Patterns in Modern Global Precipitation. *Climate Change in Continental Isotopic Records*, *78*, 1–36. doi: 10.1029/GM078p0001

Salati, E., Dall'Olio, A., Matsui, E., & Gat, J. R. (1979). Recycling of water in the Amazon Basin: An isotopic study. *Water Resources Research*, *15*(5), 1250–1258. doi: 10.1029/WR015i005p01250

Sundqvist, H. (1988). Parameterization of Condensation and Associated Clouds in Models for Weather Prediction and General Circulation Simulation. In M. E. Schlesinger (Ed.), *Physically-Based Modelling and Simulation of Climate and Climatic Change* (pp. 433–461). Dordrecht: Springer Netherlands. doi: 10.1007/978-94-009-3041-4_10 van der Ent, R. J. (2016). *WAM-2layers Python.*

van der Ent, R. J., & Savenije, H. H. G. (2013, July). Oceanic sources of continental precipitation and the correlation with sea surface temperature: Precipitation and Correlation with SST. *Water Resources Research*, *49*(7), 3993–4004. doi: 10.1002/wrcr.20296

van der Ent, R. J., Wang-Erlandsson, L., Keys, P. W., & Savenije, H. H. G. (2014, December). Contrasting roles of interception and transpiration in the hydrological cycle – Part 2: Moisture recycling. *Earth System Dynamics*, *5*(2), 471–489. doi: 10.5194/esd-5-471-2014

Winnick, M. J., Chamberlain, C. P., Caves, J. K., & Welker, J. M. (2014). Quantifying the isotopic 'continental effect'. *Earth and Planetary Science Letters*, *406*, 123–133. doi: 10.1016/j.epsl.2014.09.005

Worden, Noone, D., Bowman, K., & Tropospheric Emission Spectrometer science team and data. (2007, February). Importance of rain evaporation and continental convection in the tropical water cycle. *Nature*, *445*(7127), 528–532. doi: 10.1038/nature05508

Zemp, D. C., Schleussner, C.-F., Barbosa, H. M. J., van der Ent, R. J., Donges, J. F., Heinke, J., ... Rammig, A. (2014, December). On the importance of cascading moisture recycling in South America. *Atmospheric Chemistry and Physics*, *14*(23), 13337–13359. doi: 10.5194/acp-14-13337-2014

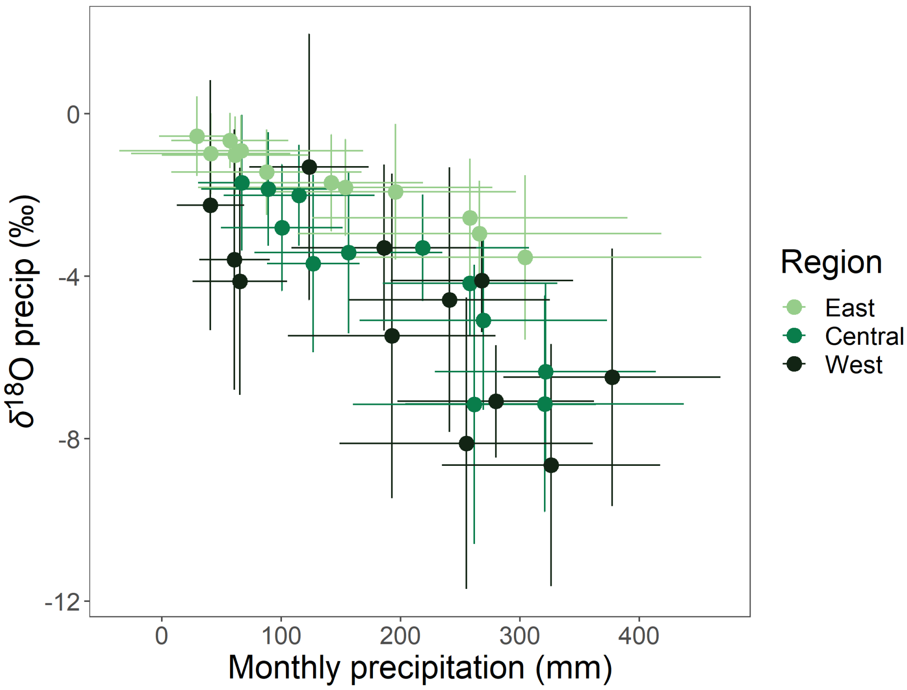

Figure S1. Relationship between $\delta^{18}O$ of modern precipitation and precipitation amount for eastern, central, and western tropical South America. All points are monthly means from GNIP. Slope of east region is similar or shallower than central and west, indicating same or larger precipitation change for the same $\delta^{18}O$. Eastern sites: Fortaleza, Ceara Mirim, Cachimbo; Central sites: Manaus, Manaus Piracicaba, Santarem; Western sites: Cruzeiro do Sul, Benjamin Constant, Porto Velho, Rio Branco.

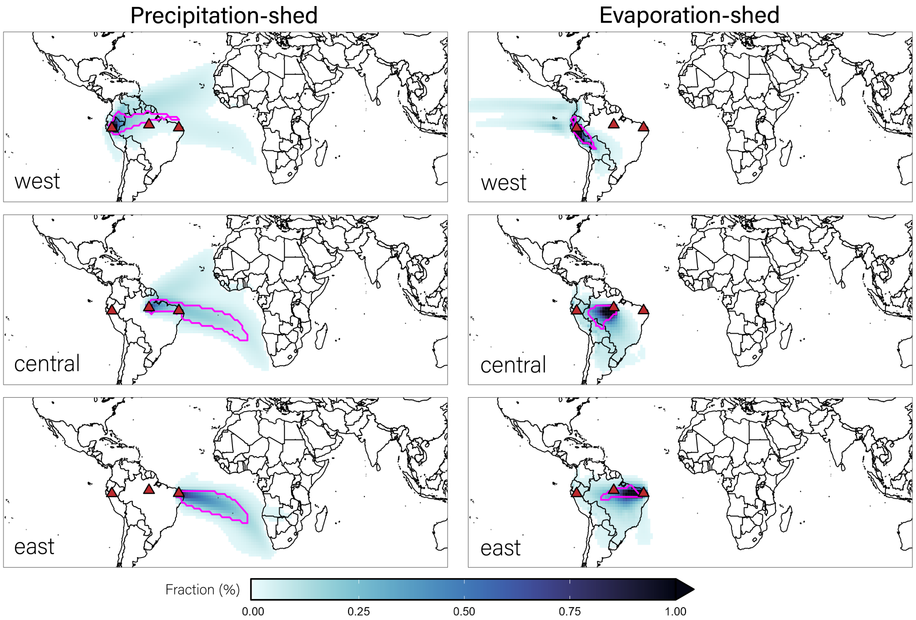

Figure S2. NDJFMAM (wet season) Two-layer WAM results using climatological mean of ERA interim reanalysis. Magenta contour line is the 70% threshold, used to indicate a dynamic connection. Note that WAM-2layers computes one round of moisture recycling, whereas some moisture likely requires more than one precipitation-evaporation cycle to reach from west to east. Generally, evaporation from upwind (east) sites is within the precipitation-shed of downwind (west) sites.

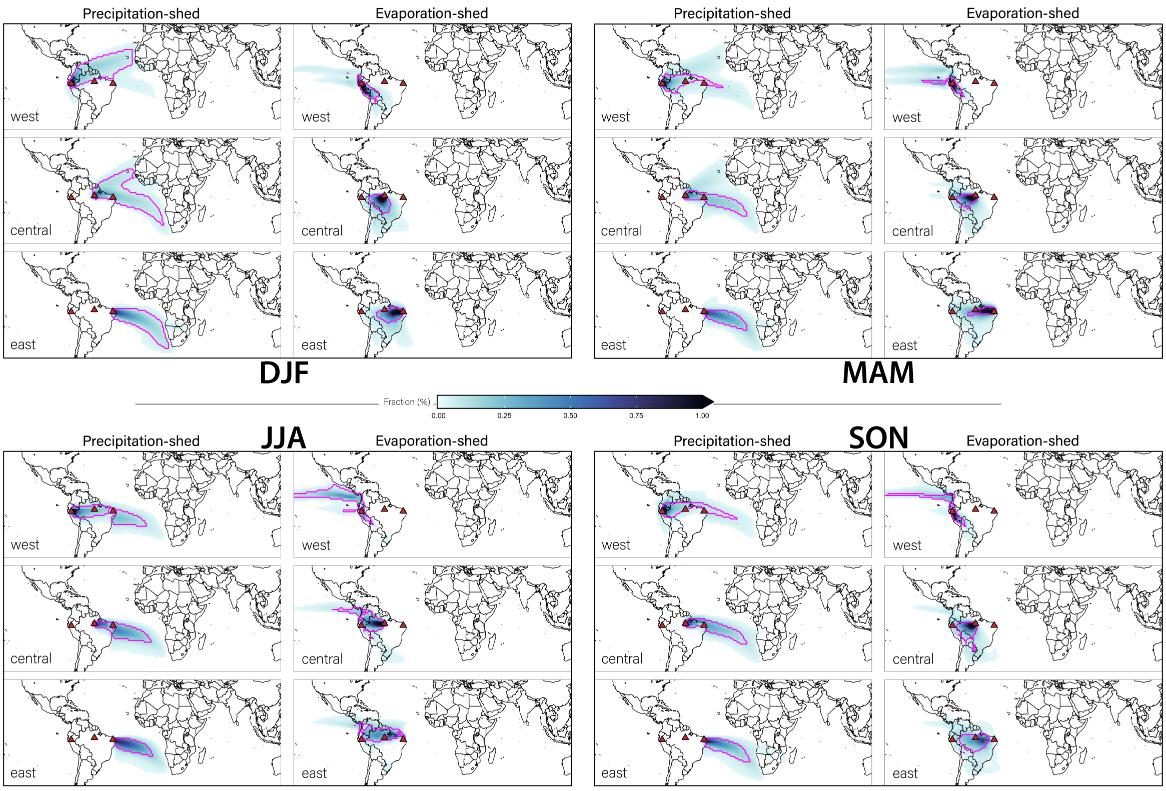

Figure S3. Seasonal Two-layer WAM results using climatological mean of ERA interim reanalysis. Same as above, but separated by season. DJF is December, January, February; MAM is March, April, May; JJA is June, July, August; and SON is September, October, November.

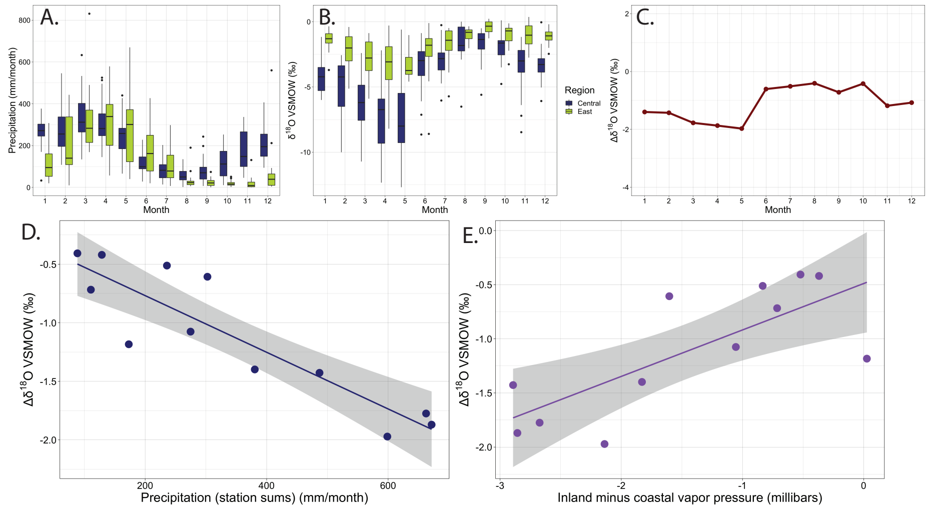

Figure S4. (**A**) Monthly precipitation rates for the Manaus GNIP station (closest to central $\delta^{18}O$ record; purple) and the Fortaleza station (closest to eastern $\delta^{18}O$ record; green). (**B**) Same as A but the isotopic composition of rainfall. (**C**) The isotope gradient between the two stations throughout the year. (**D**) Negative correlation between the isotope gradient and the sum of station precipitation indicates "amount effect"-type relationships hold across the domain on a seasonal basis. (**E**) Positive correlation between the isotope gradient and the vapor pressure difference indicates that a greater change in $\delta^{18}O$ tracks a greater change in the vapor pressure (vapor pressure values are corrected to account for an annually higher background vapor pressure in the more humid central site). All data from GNIP.

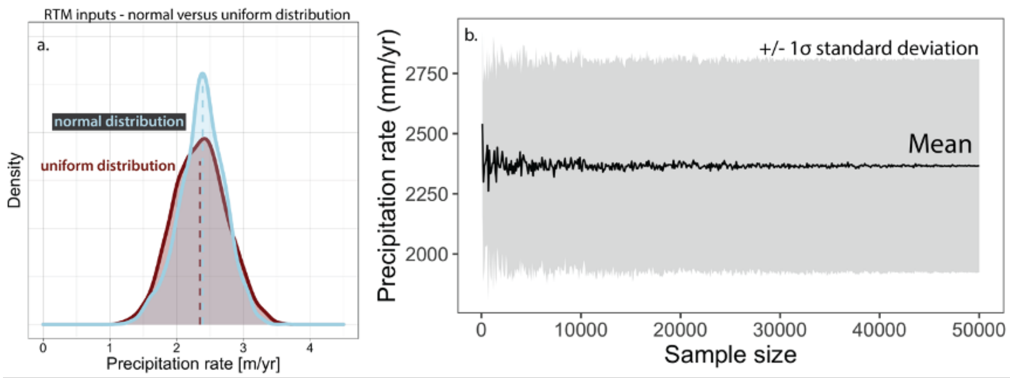

Figure S5. RTM input sensitivity and Monte Carlo diagnostics. (**A**) Comparison between assigning a uniform (dark red) versus normal (light blue) distribution to the RTM input parameters. Normal distribution leads to a narrower range of precipitation estimates. We adopt the uniform distribution for our analysis so the uncertainty on our estimates is conservative. (**B**) The mean and standard deviation of the precipitation rate stabilizes quickly, indicating the full model solution space is explored within ∼30,000 iterations.

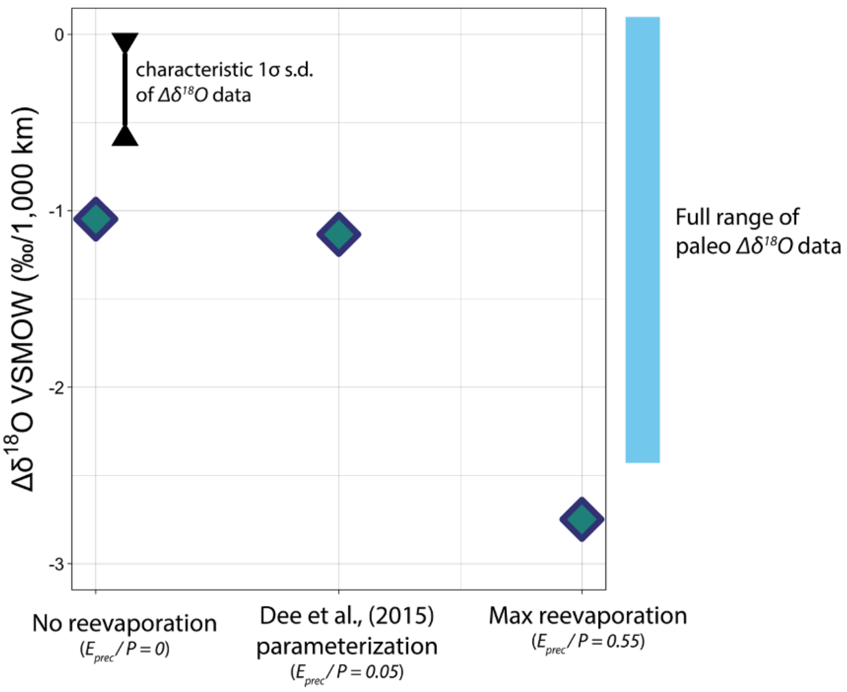

Figure S6. **Effect of re-evaporation on RTM** $\Delta\delta^{18}O$. Fractionation increases with E_{prec}/P (where E_{prec} is the evaporation flux of partially evaporated of raindrops, or raindrops whose evaporation influences $\delta^{18}O$). The isotope-based parameterization of re-evaporation in Dee et al. (2015) gives low E_{prec}/P in tropical conditions, suggesting most tropical re-evaporation (55% of P from MERRA2) has no effect on the isotopes of precipitation.

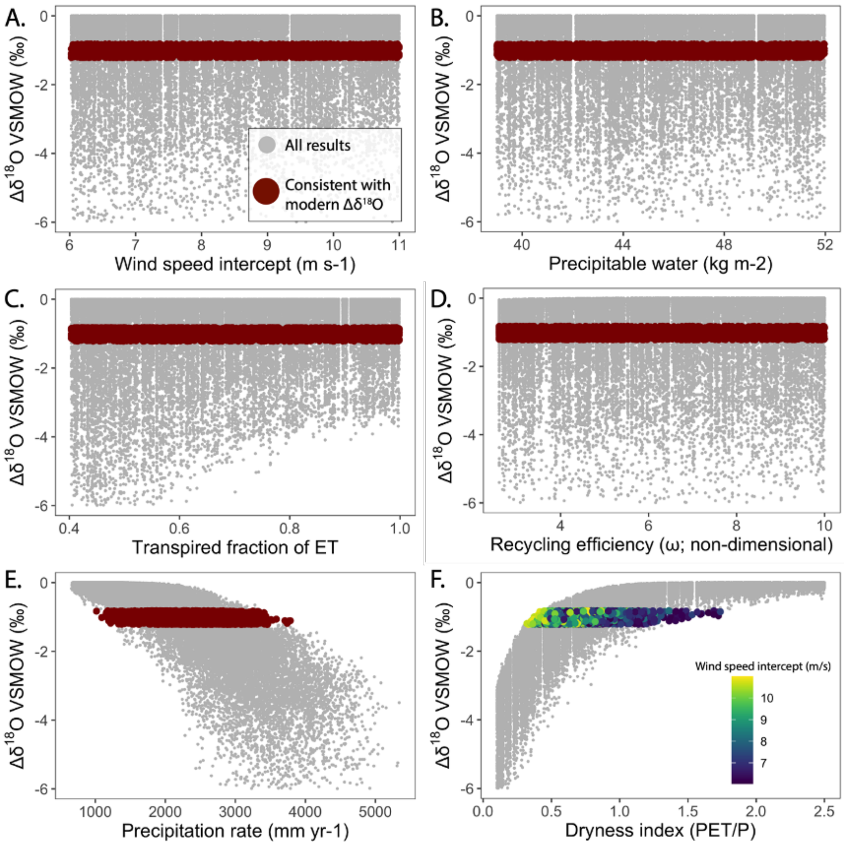

Figure S7. Monte Carlo output diagnostics for modern simulations. While all variables influence $\Delta\delta^{18}O$, opposing shifts in other terms cancel out the effect such that there is no unique solution for most variables (**A-D**). This is not the case, however, for the fluxes controlling the water balance. Both precipitation and, by consequence, the dryness index (defined as the ratio of potential ET to precipitation) have a finite set of solutions for a given $\Delta\delta^{18}O$ (**E, F**). The uncertainty in the other variables is important for building a broad, conservative uncertainty envelope in our precipitation reconstruction. For example, if we sampled a smaller range of wind speed intercepts our solution would be restricted to a smaller range of dryness indices (**F**).

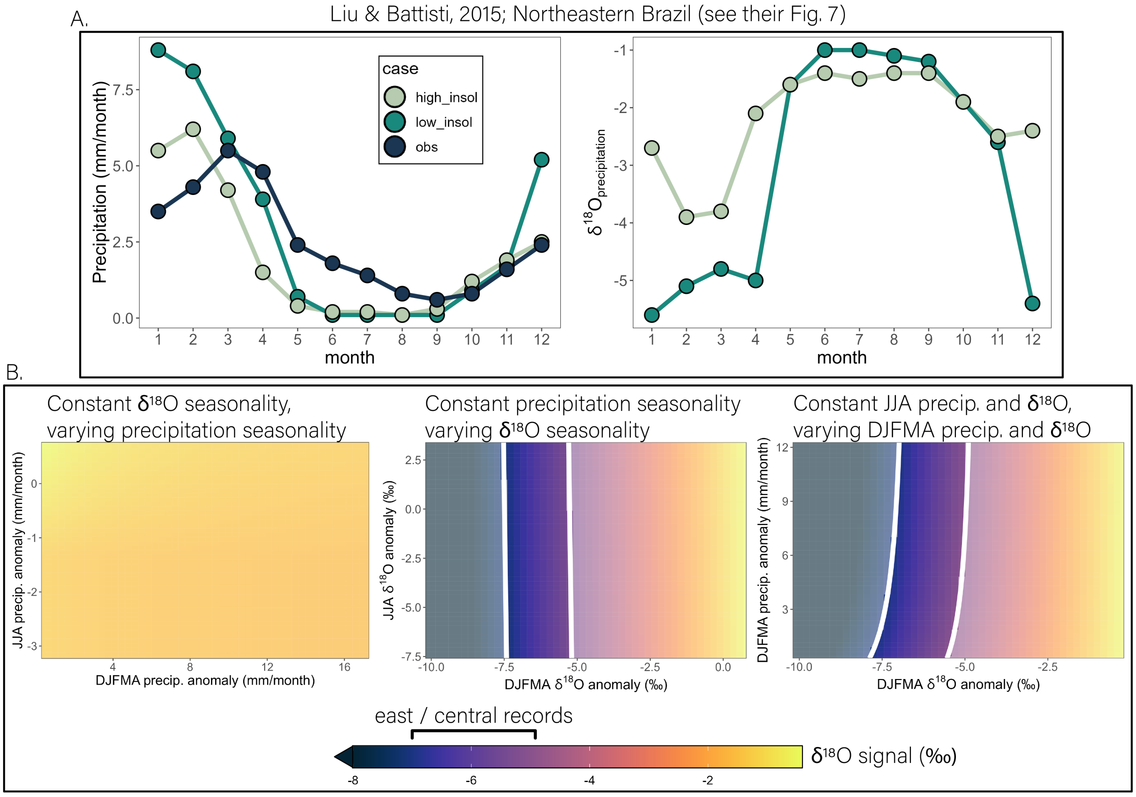

Figure S8. Changes in precipitation and $\delta^{18}O$ required to reach 5-7‰ signal with Liu & Battisti, 2015 results. (**A**) Northeastern Brazil monthly precipitation and $\delta^{18}O$ under low austral summer insolation (teal), high austral summer insolation (lightest blue), and modern observations (dark blue). Data from Fig. 7 of Liu and Battisti (2015), digitized using EngaugeDigitizer. (**B**) Effect of modifying precipitation anomaly (left), $\delta^{18}O$ anomaly (middle), or summer (DJFMA) precipitation *and* $\delta^{18}O$ anomalies (right) on the amplitude of the $\delta^{18}O$ signal. White lines denote region consistent with observations (color is grayed out outside the lines). Matching observations requires ~4x larger DJFMA $\delta^{18}O$ shift than found in simulations of Liu and Battisti (2015). The $\delta^{18}O$ signal is not very sensitive to the JJA precipitation anomaly, the JJA $\delta^{18}O$ anomaly, nor the DJF precipitation anomaly.

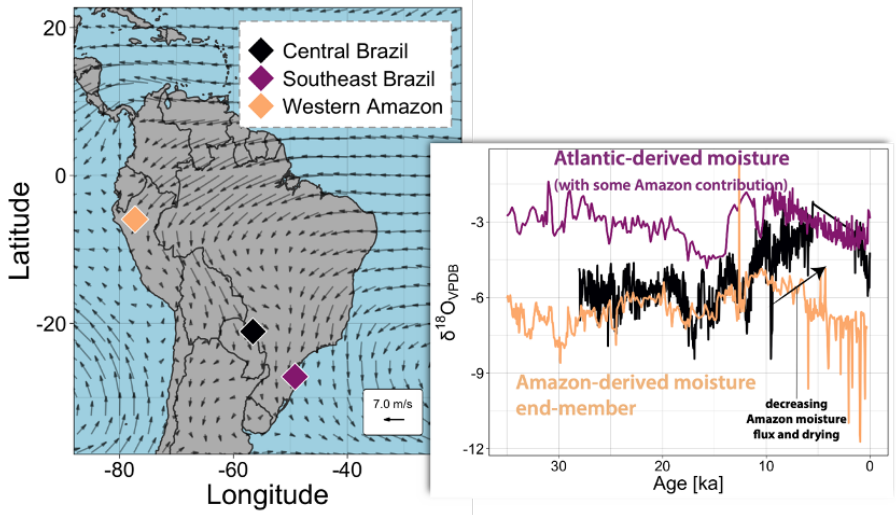

Figure S9. Amazon vs Atlantic moisture trajectories. (**Left**) Map of three speleothem sites shown in the isotope data to the right. (**Right**) Isotope records of three sites. Moisture is transported out of Amazonia from the northwesternmost site (tan diamond and line) via the Andean Low Level Jet (LLJ) to the southeasternmost site (purple diamond and line). LLJ moisture mixes with higher-$\delta^{18}O$, Atlantic-derived moisture with the maximum Atlantic contribution occurring on the coast (purple diamond). The intermediate site (black diamond and line) reflects the balance of the Amazon-derived endmember and the Atlantic endmember. $\delta^{18}O$ in the central site (black line) is similar to the Amazon-derived $\delta^{18}O$ (tan) from ~28-12 ka, indicating most precipitation comes from the LLJ. After 12 ka, $\delta^{18}O$ at the central site increases toward the southeastern (purple) values, reflecting a decrease in the LLJ moisture flux contribution as the region undergoes drying.

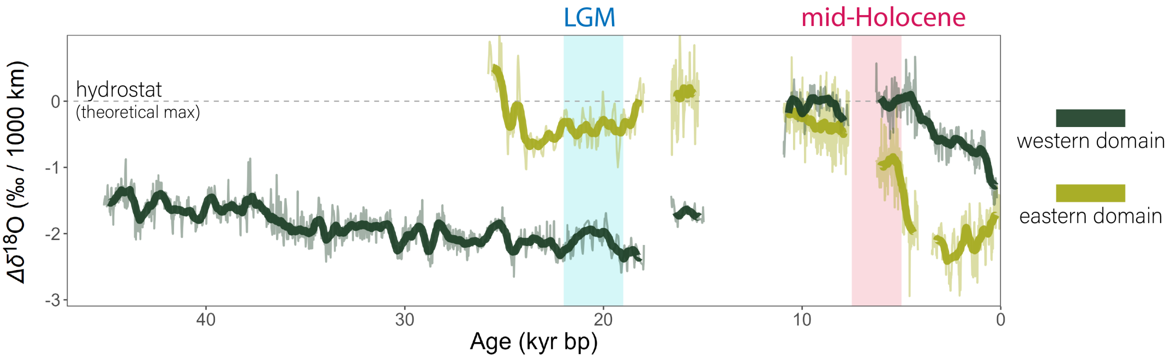

Figure S10. **Extended isotope gradient proxy record**. As in main text, but with extended western record to show lack of precession signal. More negative $\Delta\delta^{18}O$ reflects more rainout and wetter conditions. $\Delta\delta^{18}O$ of zero is the theoretical maximum value (the "hydrostat"; (Chamberlain et al., 2014; Kukla et al., 2019)) and reflects the approximate balance of P and ET.

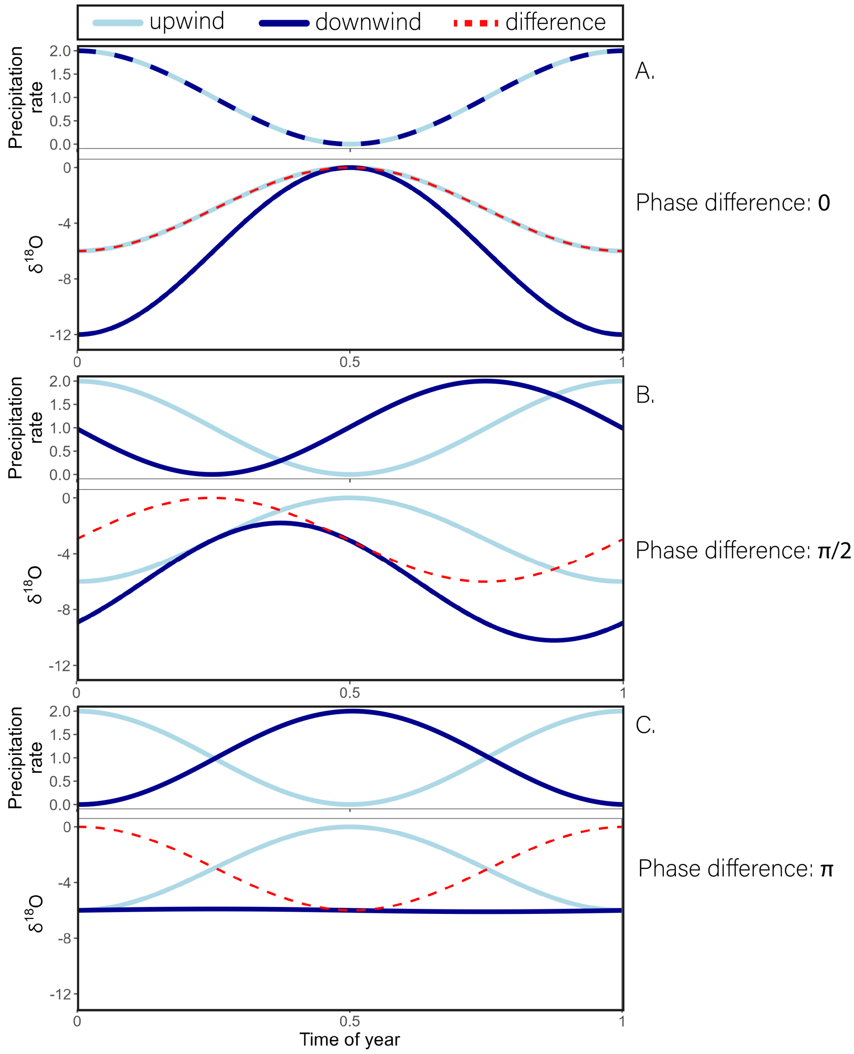

Figure S11. Precipitation and $\delta^{18}O$ for three phase differences. Results from the toy model for precipitation seasonality. Each panel (A-C) shows the annual cycle of the precipitation rate at each site (top; light blue is upwind, dark blue is downwind), and the annual cycle of $\delta^{18}O$ at each sites, as well as $\Delta\delta^{18}O$ (bottom; $\Delta\delta^{18}O$ is red dashed line). Panel (**A**) is a phase difference of zero; Panel (**B**) is a phase difference of $\frac{\pi}{2}$, or 3 months, and Panel (**C**) is a phase difference of π, or 6 months.

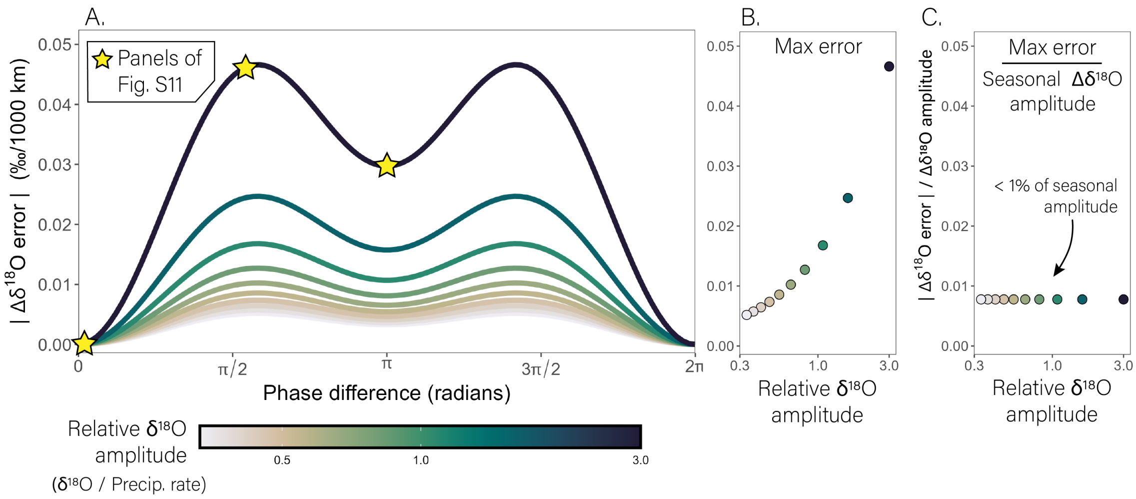

Figure S12. Sensitivity of $\Delta\delta^{18}O$ to differences in the phase of precipitation seasonality between sites. Stars denote panels in Figure S11. (**A**) Absolute $\Delta\delta^{18}O$ error (relative to no phase difference) for a phase difference of zero to 12 months (0 to 2π). Colored lines show different sensitivities of $\delta^{18}O$ to precipitation (relative $\delta^{18}O$ amplitudes). (**B**) The maximum $\Delta\delta^{18}O$ error for each relative $\delta^{18}O$ amplitude. (**C**) Maximum $\Delta\delta^{18}O$ error divided by the seasonal amplitude of $\Delta\delta^{18}O$. Relative to the seasonal $\Delta\delta^{18}O$ amplitude, the error induced by phase differences between sites is less than 1%.

The zonal patterns in late Quaternary tropical South American precipitation

T. Kukla[1,2], M. J. Winnick[3], M. M. Laguë[4,5], Z. Xia[3,6]

[1]Department of Geosciences, Colorado State University, Fort Collins, CO, USA
[2]Department of Geological Sciences, Stanford University, Stanford, CA, USA
[3]Department of Geosciences, University of Massachusetts Amherst, Amherst, MA, USA
[4]University of Saskatchewan Coldwater Lab, Canmore, Alberta, Canada
[5]Department of Atmospheric Sciences, University of Utah, Salt Lake City, UT, USA
[6]Key laboratory of Geogrpahical Processes and Ecological Security in Changbai Mountains, Ministry of Education, School of Geographical Sciences, Northeast Normal University, Changchun, China

Key Points:

- The late Quaternary South American Precipitation Dipole drives opposing east-west precipitation anomalies in tropical South America.
- Dipole transitions can drive changes in rainfall greater than 1000 mm/yr.
- Spatial migration of the precipitation centroid can explain dipole transitions and reconcile proxy-model conflicts.

Corresponding author: Tyler Kukla, `tykukla@colostate.edu`

Abstract

Speleothem oxygen isotope records ($\delta^{18}O$) of tropical South American rainfall in the late Quaternary show a zonal "South American Precipitation Dipole" (SAPD). The dipole is characterized by opposing east-west precipitation anomalies compared to the present—wetter in the east and drier in the west at the mid-Holocene (∼7 ka), and drier in the east and wetter in the west at the Last Glacial Maximum (LGM; ∼21 ka). However, the SAPD remains enigmatic because it is expressed differently in western versus eastern $\delta^{18}O$ records and isotope-enabled climate model simulations usually misrepresent the magnitude and/or spatial pattern of $\delta^{18}O$ change. Here, we address the SAPD enigma in two parts. First, we re-interpret the $\delta^{18}O$ data to account for upwind rainout effects that are known to be pervasive in tropical South America, but are not always considered in Quaternary paleoclimate studies. Our revised interpretation reconciles the $\delta^{18}O$ data with cave infiltration and other proxy records, and indicates that the centroid of tropical South American rainfall has migrated zonally over time. Second, using an energy balance model of tropical atmospheric circulation, we hypothesize that zonal migration of the precipitation centroid can be explained by regional energy budget shifts, such as changing Saharan albedo associated with the African Humid Period, that have not been modeled in previous SAPD studies. This hypothesis of a migrating precipitation centroid presents a new framework for interpreting $\delta^{18}O$ records from tropical South America and may help explain the zonal rainfall anomalies that predate the late Quaternary.

Plain Language Summary

Paleoclimate data suggest that, in the last ∼25 thousand years, tropical South American precipitation has changed substantially, but in opposite directions between the east and west. This opposing east-west pattern in past rainfall is known as the "South American Precipitation Dipole", and its end-member states approximately coincide with the Last Glacial Maximum (∼21 thousand years ago) and mid-Holocene (∼7 thousand years ago), respectively. However, the cause of the dipole is debated because different models produce different results, and the interpretations of data are in conflict. Central in this conflict are oxygen isotope tracers of past precipitation which show different trends over space. We present a new interpretation of these data, backed by model results, which suggests that the dipole is driven by the centroid, or focus, of tropical South American precipitation migrating from west-to-east (and back) across tropical South America. We test this precipitation centroid migration hypothesis with an energy balance climate model which reproduces the expected east-west differences for the Last Glacial Maximum and mid-Holocene. The precipitation centroid migration hypothesis is a possible solution to the precipitation dipole enigma, but it remains to be tested in more sophisticated climate models.

1 Introduction

Tropical South America spans about one-tenth of the Earth's circumference from east to west (zonally). There is mounting evidence that rainfall across this stretch has varied in a zonal "dipole" fashion in the late Quaternary (here, the last ∼25 kyr) with rainfall increasing in northeastern Brazil at the expense of drying in western Amazonia, and vice versa (Martin et al., 1997; Cruz et al., 2009; Cheng et al., 2013; M. C. Campos et al., 2022). This zonal rainfall pattern is called the "South American Precipitation Dipole" (SAPD), a term that describes the opposing east-west patterns of past rainfall anomalies (Fig. 1a,b), and is distinct from the precipitation dipole studied in the modern climate between southeastern South America and the South Atlantic Convergence Zone (Nogués-Paegle & Mo, 1997; Boers et al., 2014). The SAPD has been identified on precession (Martin et al., 1997; Wang et al., 2004; Cruz et al., 2009; Cheng et al., 2013) and glacial-interglacial timescales (Abouchami & Zabel, 2003; Mason et al., 2019), and it corresponds with many high-amplitude signals in paleoclimate proxy data (P. A. Baker, Seltzer, et al., 2001; P. A. Baker, Rigsby, et al., 2001; Tapia et al., 2003; Fritz et al., 2004; Cruz et al., 2009; Wang et al., 2017). Still, conflicting model and proxy interpretations cast doubt on what drives the SAPD (Cruz et al., 2009; Liu & Battisti, 2015; M. C. Campos et al., 2022), and even whether it exists at all (Wang et al., 2017).

On precession timescales, a primary challenge of the SAPD enigma is how to interpret the speleothem oxygen isotope ($\delta^{18}O$) records that span the dipole region (Fig. 1c-e). These spatially and temporally complex $\delta^{18}O$ records are difficult to reconcile with some independent proxy data. From the relatively high austral summer insolation phase around the Last Glacial Maximum (LGM; ∼20 ka) to the lower phase at the mid-Holocene (∼7 ka), the speleothem $\delta^{18}O$ records are zonally imbalanced—the $\delta^{18}O$ shifts to the east are about twice as large as the opposing shifts in the west. East $\delta^{18}O$ is, if anything, less sensitive to precipitation amount than west $\delta^{18}O$ today (Fig. S1), so it is speculated that these data imply a zonally imbalanced SAPD with larger precipitation anomalies in the east (Cheng et al., 2013). Yet, the implication of a more quiescent precipitation history in the west is not consistent with previous evidence for substantial drying from the wetter-than-present LGM to the mid-Holocene (P. A. Baker, Seltzer, et al., 2001; P. A. Baker, Rigsby, et al., 2001; Fritz et al., 2004; Tapia et al., 2003). Further, evidence from strontium isotopes in speleothems across tropical South America shows $\delta^{18}O$ is often decoupled from rainfall amount (Wortham et al., 2017; Ward et al., 2019). Thus, it is not clear that zonally imbalanced $\delta^{18}O$ signals require a zonally imbalanced SAPD.

The speleothem $\delta^{18}O$ data also reveal important discrepancies with isotope-enabled General Circulation Models (GCMs) forced with precession. In isotope-enabled GCMs, opposing east-west precipitation and $\delta^{18}O$ anomalies have a similar magnitude—the SAPD is zonally balanced (Cruz et al., 2009; Liu & Battisti, 2015). Under low summer insolation, precipitation $\delta^{18}O$ decreases by 1-3‰ in the east, increases by the same amount in the west, and shows no change in east-central Amazonia where there is a large ∼6‰ shift in the speleothem data (Cruz et al., 2009; Liu & Battisti, 2015; Wang et al., 2017). Thus, while the direction of change is reasonable, the magnitude and spatial pattern of $\delta^{18}O$ is inconsistent with the speleothem data, suggesting factors other than precession may contribute to the late Quaternary SAPD. Precession may also be insufficient to explain the apparent out-of-phase changes in speleothem $\delta^{18}O$ in the last ∼15 kyr (Fig. 1c-e). Precession-driven insolation forcing is uniform east-to-west, but minimum and maximum $\delta^{18}O$ values occur at different times across tropical South America.

The goal of this manuscript is to develop a conceptual model for the late Quaternary SAPD that is consistent with the enigmatic features of the oxygen isotope records—namely the zonally imbalanced $\delta^{18}O$ signals and their out-of-phase nature. We begin by reinterpreting the $\delta^{18}O$ data to account for the effect of upwind rainout (where upwind is east). Upwind rainout can decouple local $\delta^{18}O$ from local rainfall amount by generating low-$\delta^{18}O$ moisture that is transported downwind. The effect is widely known to drive Amazon $\delta^{18}O$ in modeling, observational, and paleoclimate studies (Salati et al., 1979; Grootes et al., 1989; Gat & Matsui, 1991; Vuille et al., 2003; Vimeux et al., 2005; Vuille & Werner, 2005; Brienen et al., 2012; J. C. A. Baker et al., 2016; Ampuero et al., 2020), yet has not been empirically constrained in previous interpretations of the SAPD (van Breukelen et al., 2008; Cruz et al., 2009; Cheng et al., 2013). Accounting for upwind rainout yields two important results. First, it brings the $\delta^{18}O$ data in better agreement with other proxy records, including strontium isotopes, and casts the SAPD as zonally balanced—the magnitude of precipitation anomalies is similar in the east and west. Second, the $\delta^{18}O$ data can be understood as recording zonal shifts in the location of maximum rainout, or the "precipitation centroid", across tropical South America. A precipitation centroid that migrates east-west reconciles a zonally balanced SAPD with zonally imbalanced $\delta^{18}O$ anomalies and it explains the out-of-phase $\delta^{18}O$ signals. Yet, the mechanisms for a zonally migrating precipitation centroid are not immediately clear.

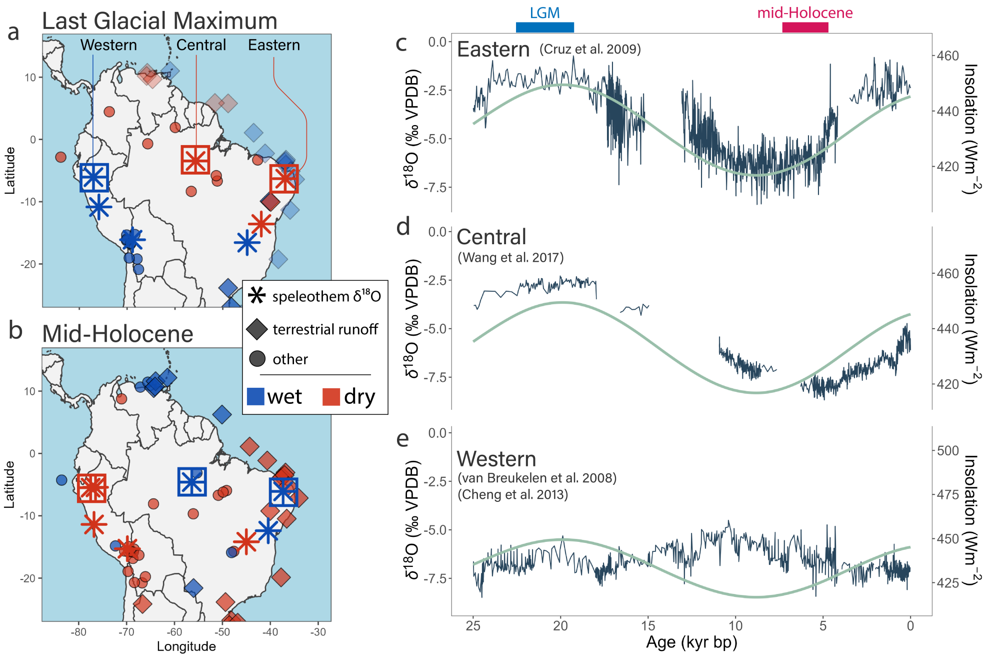

Figure 1. South America proxy map and isotope data. Proxy map for the LGM (∼21 ka) (**A**) and mid-Holocene (∼7 ka) (**B**). Data points in **A** and **B** are jittered to show instances of multiple proxy records from the same site. Offshore runoff proxies are lighter in panel A because they can record a sea-level signal at the Last Glacial Maximum. (**C**) Rio Grande do Norte (eastern) $\delta^{18}O$ record (Cruz et al., 2009). (**D**) Paraíso (central) $\delta^{18}O$ record (Wang et al., 2017). (**E**) Diamante and Tigre Perdido composite (western) $\delta^{18}O$ record (van Breukelen et al., 2008; Cheng et al., 2013). Teal lines (**C-E**) show February insolation at 10°S following Cruz et al. (2009) (scales varied to match $\delta^{18}O$ magnitude).

In the second part of our analysis, we test whether precession forcing can explain a migrating precipitation centroid. Precession is considered the primary driver of the SAPD, and it was previously linked to east-west shifts in the pan-Asian Monsoon precipitation centroid (Battisti et al., 2014). These zonal pan-Asian Monsoon shifts caused large changes in $\delta^{18}O$ and precipitation, and we find similarly large changes in South America using an isotope-enabled reactive transport model (Kukla et al., 2019). However, the same GCM simulations presented in Battisti et al. (2014) showed no zonal migration in the tropical South American precipitation centroid, and we also find no zonal shifts in the PMIP3/CMIP5 models. Instead, we posit that land surface albedo change, in addition to precession, can explain the late Quaternary SAPD. We impose reasonable late Quaternary land albedo forcings in an energy balance model for tropical atmospheric circulation and find zonal shifts in the South American precipitation centroid that are consistent with the isotope data. We conclude that, while precession can drive a zonal precipitation dipole, additional forcings such as land albedo are necessary to explain the zonal imbalance of $\delta^{18}O$ signals, their magnitude, and their out-of-phase trends.

2 Late Quaternary speleothem $\delta^{18}O$ records and precipitation dynamics

Our analysis leverages three existing speleothem $\delta^{18}O$ records that span tropical South America and have previously been used to identify the SAPD. We refer to these as the eastern, central, and western records (Fig. 1). The eastern record is from the Rio Grande do Norte site of northeastern Brazil and shows a 5-7‰ decrease in $\delta^{18}O$ from the LGM to early-mid Holocene interpreted as evidence for a weakening South American Monsoon (Cruz et al., 2009) (Fig. 1c). The central record comes from the Paraíso site in east-central Amazonia (Wang et al., 2017) and resembles the eastern record, but the $\delta^{18}O$ decrease lags behind by 1-2 kyr, and the records diverge in the late Holocene (Fig. 1d). Given its location near the monsoon's deep convective region, data from the central site were interpreted as evidence for stronger convection in the mid-Holocene, in conflict with the eastern record interpretation (Wang et al., 2017). The western record is a composite of the Diamante (Cheng et al., 2013) and Tigre Perdido (van Breukelen et al., 2008) records (Fig. 1e). We adopt the cave temperature correction for these records following Wang et al. (2017) (see also Ampuero et al. (2020); Kukla et al. (2021)), increasing $\delta^{18}O$ by 1.4‰ to account for its relatively cooler cave temperatures. These records are interpreted to reflect Amazon or western Amazon rainfall amount, with a muted $\delta^{18}O$ increase of $\sim$2.5‰ from the LGM to early Holocene indicative of drying, then a gradual decrease to wetter, present conditions that starts when the eastern and then central $\delta^{18}O$ records initially decrease. The western record stands out from the central and eastern records in that $\delta^{18}O$ increases, rather than decreases, from the LGM to the early-mid Holocene. This contrast defines the $\delta^{18}O$ expression of the SAPD, with the western-wet phase at the LGM and eastern-wet phase at the mid-Holocene representing end-member SAPD states.

The zonal SAPD is likely driven by multiple factors but, on precession timescales, it is agreed that changes in austral summer insolation are critical (Cruz et al., 2009; Cheng et al., 2013; Prado et al., 2013; Liu & Battisti, 2015; M. C. Campos et al., 2022). Precession drives summer insolation with a $\sim$21 kyr beat, and this forcing carries no zonal component. Low austral summer insolation (as during the mid-Holocene, $\sim$7 ka) weakens the South American Monsoon and decreases rainfall in western tropical South America (P. A. Baker, Seltzer, et al., 2001; Cruz et al., 2009; Liu & Battisti, 2015; M. C. Campos et al., 2022). However, the opposing increase in eastern precipitation requires some zonal shift in atmospheric circulation, and the cause is debated. One theory posits that weaker subsidence over northeast Brazil must compensate for weaker convection to the west, increasing northeast Brazil rainfall (Cruz et al., 2009; Shimizu et al., 2020; M. C. Campos et al., 2022). Another argues that northeast Brazil rainfall increases as south African summer cooling shifts the subtropical rain band, the South Atlantic Convergence Zone, northward, and north African cooling shifts the tropical rain band, the Inter-Tropical Convergence Zone (ITCZ), southward (Liu & Battisti, 2015), consistent with a broader seasonal ITCZ migration (Chiessi et al., 2021). In both cases models capture zonally opposing $\delta^{18}O$ anomalies, but not their zonal imbalance, nor the magnitude of eastern and central $\delta^{18}O$ change (note that the central record was published after Cruz et al. (2009) and Liu and Battisti (2015)). Moreover, other simulations with precession forcing find no SAPD, or a zonal precipitation dipole in the austral summer that is offset by opposing anomalies in the austral winter (Prado et al., 2013; Tigchelaar & Timmermann, 2016; Shimizu et al., 2020). One key limitation in the application of these models to the mid-Holocene is they do not account for the greening-induced decrease in Saharan land albedo—a major boundary condition change that has previously been linked to rainfall anomalies in tropical South America (Lu et al., 2021). If such zonal forcings can impact tropical South American rainfall, they may be critical for explaining the zonal patterns of the SAPD.

Recent theoretical work demonstrates that South American rainfall, more so than other tropical regions, is energetically primed to shift east-west due to factors like non-local land surface albedo change (Boos & Korty, 2016). The precipitation centroid in tropical South America sits at the intersection of the energy flux equator (correlated with the ITCZ) and an energy flux prime meridian (Boos & Korty, 2016). These energy flux lines occur where column-integrated divergent atmospheric energy transport is zero in the meridional (energy flux equator) and zonal (energy flux prime meridian) directions (Boos & Korty, 2016). The energy flux equator-prime meridian intersection conditions the precipitation centroid to migrate zonally because, just as the energy flux equator (and ITCZ) moves north and south following anomalous meridional energy sources (*e.g.*, changes in insolation and albedo), the energy flux prime meridian moves west and east in response to zonal energy anomalies. North-south shifts in the precipitation centroid, following the energy flux equator, are well documented in tropical South America and elsewhere (Haug, 2001; Arbuszewski et al., 2013; Deplazes et al., 2013; Mulitza et al., 2017; J. L. P. S. Campos et al., 2019; Chiessi et al., 2021), but east-west shifts are less thoroughly explored. The pan-Asian monsoon is also associated with an energy flux prime meridian and has been shown to migrate zonally with high-amplitude precession forcing, though precession alone appears insufficient to shift the precipitation centroid east-west in South America (Battisti et al., 2014; Liu & Battisti, 2015; Shimizu et al., 2020). If other factors drove the energy flux prime meridian over South America to shift zonally in the past, we expect the precipitation centroid to shift with it (Boos & Korty, 2016), driving a zonal dipole in rainout expressed as the SAPD.

3 Methods

3.1 Paleo-isotope gradient justification

The isotope gradient is defined as downwind $\delta^{18}O$ minus upwind $\delta^{18}O$ along a given moisture trajectory and it is expressed in units of ‰ per thousand kilometers. This change in $\delta^{18}O$ is related to Rayleigh distillation interpretations of isotopic data as both $\delta^{18}O$ and $\Delta\delta^{18}O$ decrease as net rainout (or distillation) increases (Salati et al., 1979; Gat & Matsui, 1991). Whereas one must assume the upwind $\delta^{18}O$ value to interpret a given $\delta^{18}O$ record in terms of net rainout, $\Delta\delta^{18}O$ explicitly accounts for these upwind variations, theoretically isolating the $\delta^{18}O$ signal due to rainout alone (Hu et al., 2008; Winnick et al., 2014; Kukla et al., 2019, 2021). This approach is particularly useful in tropical South America because upwind effects are known to be a primary driver of $\delta^{18}O$ (Salati et al., 1979; Gat & Matsui, 1991; Vuille et al., 2003; Vuille & Werner, 2005; Lee et al., 2009; Liu & Battisti, 2015; J. C. A. Baker et al., 2016; Ampuero et al., 2020). Upwind and local rainout can be distinguished because upwind rainout will change the initial $\delta^{18}O$ of a given domain but not $\Delta\delta^{18}O$ (Salati et al., 1979; Kukla et al., 2021). We note that $\Delta\delta^{18}O$ values are generally restricted to below zero (the "hydrostat"), since a zero isotope gradient reflects all precipitation being recycled between two sites or zero or negligible precipitation (i.e. no net rainout) (Caves et al., 2015; Chamberlain et al., 2014; Kukla et al., 2019).

To validate our use of the isotope gradient approach, we analyze the connectivity of atmospheric moisture through transport and recycling among the eastern, central, and western sites in the modern climate. We use the 2-layer Water Accounting Model (WAM-2layers) (van der Ent et al., 2014) and the precipitation back-tracking scheme of Keys et al. (2012) (van der Ent & Savenije, 2013; van der Ent, 2016). The model simulates precipitation-sheds, the area where evaporation sources a site's precipitation, and evaporation-sheds, the area where a site's evaporation re-precipitates out. Contours enclosing the area where 70% of a site's rainfall is sourced (for precipitation-sheds) or a site's evaporation rains out (for evaporation-sheds) can be used to infer a meaningful dynamic connection between sites (Keys et al., 2012). We find that moisture recycling between our sites surpasses this threshold (Fig. 2), demonstrating that these sites are sufficiently isotopically connected for $\Delta\delta^{18}O$ analysis (see Supplemental Text S1; Fig. S2, S3). We also find that the modern isotope gradient across tropical South America is negatively correlated with rainout and is negative throughout the year, consistent with theory for upwind signals propagating downwind with minimal attenuation (Fig. S4) (Kukla et al., 2019). Constraining the isotopic connectivity between sites is challenging, in part because a strong connection today does not necessarily imply a strong connection in the past. Yet, as air-

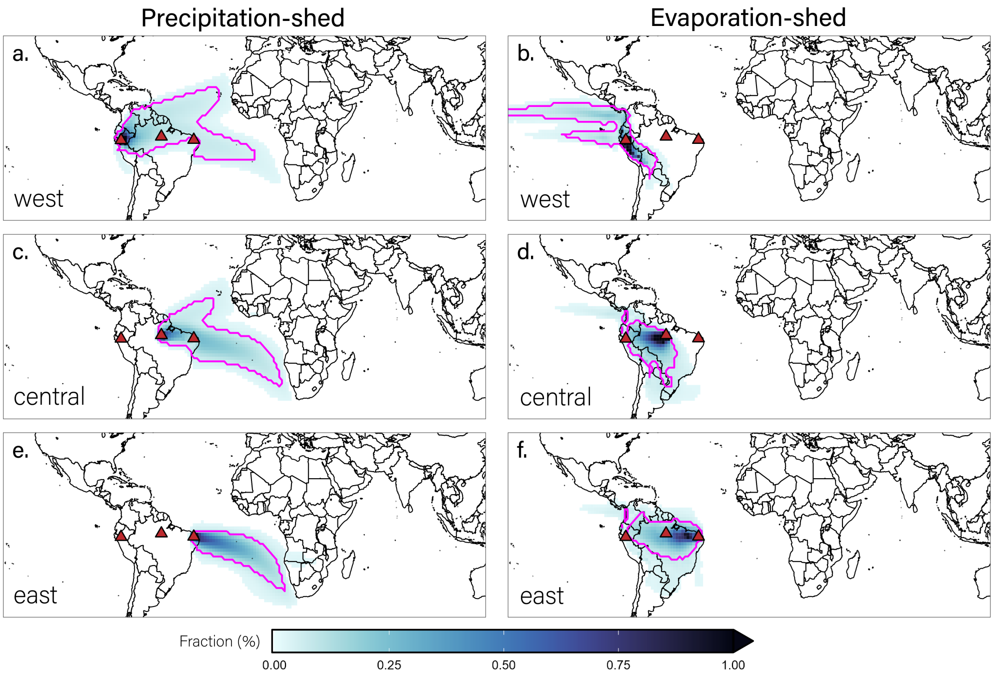

Figure 2. WAM-2layers hydrologic connectivity between speleothem sites. Annual mean precipitation-sheds (A, C, E) and evaporation-sheds (B, D, F) for the western (**A, B**), central (**C, D**), and eastern (**E, F**) sites. Magenta line denotes the spatial threshold where 70% of precipitation is sourced (precipitation-sheds) or where evaporation re-precipitates (evaporation-sheds), used to indicate a dynamically significant connection (Keys et al., 2012). Results show sites are significantly hydrologically connected within a single evaporation-precipitation cycle (See supplement for seasonal results).

masses shift in response to past forcings, moisture at one site can still be recycled to the next. Today, moisture recycling connects regions across tropical South America that receive their peak rainfall at different times of the year (Staal et al., 2018). We discuss how weak isotopic connections would affect our conclusions in section 5.4.

3.2 Reconstructing paleo-precipitation rates from the central-to-western sites

We focus exclusively on the isotope gradient between the central and western sites for our quantitative precipitation reconstruction because this trajectory aligns best with that of the prevailing winds (see Supplemental Text S1, S2). Oxygen isotope gradients along a dominant moisture trajectory depend on the balance of three fluxes: precipitation, evapotranspiration, and atmospheric transport (Salati et al., 1979; Winnick et al., 2014). We use a reactive transport model that simulates $\Delta\delta^{18}O$ as a function of these fluxes to quantify past precipitation rates from $\Delta\delta^{18}O$ data. To do so, we randomly sample from uniform distributions of reactive transport model input parameters to estimate past precipitation from the simulations that agree with $\Delta\delta^{18}O$ data (Kukla et al., 2019, 2021).

Our application of the reactive transport model to the central-to-western isotope gradient follows that of Kukla et al. (2021) with one key change. Kukla et al. (2021) used modern reanalysis data to analyze both the late Holocene and mid-Holocene isotope gradients because PMIP3/CMIP5 results (Braconnot et al., 2012) show that reactive transport model inputs are similar for both time periods. However, modern reanalysis data cannot be reasonably applied to the LGM due to the $\sim$5°C of tropical cooling. To account for this cooling, we apply temperature-based scaling relationships to the reanalysis data to estimate LGM moisture content over the ocean (moisture source region) and potential evapotranspiration. Source region moisture content is calculated assuming relative humidity remains constant over the ocean (Sherwood et al., 2010), and potential evapotranspiration is decreased following the scaling relationship defined by Scheff and Frierson (2014) and Siler et al. (2019). Decreasing source moisture content and potential evapotranspiration both increase net rainout, all else equal. Therefore, these changes decrease the reconstructed LGM precipitation rates required to reproduce a given isotope gradient. Moisture content and humidity are allowed to change over land depending on model-simulated rainout. We further account for unique LGM conditions by restricting the wind speed and transpiration fraction estimates. Proxy studies (McIntyre & Molfino, 1996; Bradtmiller et al., 2016; Venancio et al., 2018) suggest that the northeasterlies were stronger at the LGM, so we restrict wind speeds to be equal to or greater than the late Holocene. Lower atmospheric pCO_2 implies lower plant water use efficiency suggesting that more transpiration may have been necessary to fix (approximately) the same amount of carbon. Since the rainforest largely remained intact at the LGM (*i.e.* similar biomass), we assume the transpired fraction of evapotranspiration is also equal to or greater than modern.

We find that our results are not sensitive to the shape of the distributions of model inputs, nor the sample size of the Monte Carlo routine (Fig. S5). We also test the importance of an additional input, rain re-evaporation, on model $\delta^{18}O$. Rain re-evaporation and its effect on $\delta^{18}O$ is heavily parameterized in models because it is difficult to directly measure (Worden et al., 2007; Dee et al., 2015; Konecky et al., 2019) (see Supplementary text S2-S3). Using a parameterization fit to isotope data we find that it has a negligible effect on $\delta^{18}O$ in the model (Fig. S6). Diagnostics of our late Holocene Monte Carlo results (essentially a modern analysis because late Holocene speleothem $\Delta\delta^{18}O$ is the same as modern rainfall) are provided in Fig. S7.

We further use the reactive transport model to calculate spatial $\delta^{18}O$ patterns for individual PMIP3/CMIP5 models (Braconnot et al., 2012). Using zonal profiles of atmospheric moisture content, zonal winds, potential evapotranspiration, and temperature from the individual PMIP3/CMIP5 models, we run the reactive transport model to simulate the isotope gradient for the LGM, mid-Holocene, and late Holocene (PMIP3/CMIP5 pre-industrial). We then compare the predicted $\Delta\delta^{18}O$ derived from the PMIP3/CMIP5 data to the speleothem data. If the predicted $\Delta\delta^{18}O$ is more negative than the observed $\Delta\delta^{18}O$, then the net rainout in that model is too high to reconcile the observed data in the reactive transport framework. We also analyze the precipitation rate necessary to match the paleo-isotope gradient if all other PMIP3/CMIP5 inputs to the reactive transport model are correct. This analysis effectively asks how much rainfall must increase or decrease relative to the PMIP3/CMIP5 prediction in order to reconcile the paleoclimate $\Delta\delta^{18}O$ data.

3.3 Application of a 2-dimensional atmosphere energy balance model

We use a 2-dimensional energy balance model that is capable of tracking zonal shifts in the precipitation centroid (Boos & Korty, 2016) to accomplish two related goals. First, we identify the precipitation centroid to test whether it shifts zonally in the mid-Holocene or LGM simulations of the PMIP3/CMIP5 models. Second, we simulate the zonal precipitation centroid response to conditions that likely characterize the LGM and mid-Holocene but are not accounted for in the PMIP3/CMIP5 experiments.

The energy balance model predicts how changes in energy input to the atmosphere would change atmospheric energy transport, thus altering atmospheric circulation and precipitation patterns. Here, we follow the methodology of Boos and Korty (2016) and consider how changes in continental albedo alter energy input to the atmosphere, and how atmospheric circulation would have to adjust in order to maintain the energy balance. The anomalous energy flux generated by the energy balance model is then used to infer a shift in precipitation based on the assumption that the position of peak precipitation migrates with the intersection of the energy flux equator and energy flux prime meridian (see equations 2-7 in Boos and Korty (2016)). We refrain from attributing the precipitation centroid anomalies to a specific atmospheric feature because the model is not designed to distinguish between the individual effects of, for example, the South American Monsoon, the South Atlantic Convergence Zone, and the ITCZ.

3.3.1 Analysis of PMIP3/CMIP5 precipitation dynamics

Using the energy balance model, we identify the PMIP3/CMIP5 ensemble mean location of the precipitation centroid, defined as the intersection of the energy flux equator and prime meridian, for the LGM, mid-Holocene, and pre-industrial (or late Holocene). The LGM and mid-Holocene ensemble means are then used as the initial conditions for the perturbations discussed in the next section.

3.3.2 Simulating additional LGM and mid-Holocene constraints

A critical step in determining whether the precipitation centroid migrated zonally in the past is quantifying the sensitivity of zonal shifts to energetic forcing. We impose anomalous moist static energy sources in the PMIP3/CMIP5 ensemble mean to quantify how the zonal location of the energy flux prime meridian (and thus the precipitation centroid (Boos & Korty, 2016)) changes with zonal forcing. The response of the South American precipitation centroid to anomalous energy forcing depends on (*1*) the magnitude and direction of energetic forcing; (*2*) the area over which the forcing is applied; and (*3*) the distance (especially zonally) of the anomalous forcing to the centroid.

During the mid-Holocene, lower land surface albedo likely increased the net column energy over the grassy "green" Sahara by about 70 W/m^2, accounting for the attenuation of the albedo anomaly at the top of the atmosphere (Boos & Korty, 2016). This forcing exceeds the magnitude of insolation change due to orbital variability ($\sim$10 W/m^2 in the mid-Holocene), but is applied over a smaller area (confined to the modern Sahara). Other modeling investigations of the late Quaternary SAPD (including PMIP3/CMIP5 simulations) accounted for orbital forcing, but did not consider the Green Sahara (Cruz et al., 2009; Liu & Battisti, 2015). During the LGM there is evidence for forest dieback and grassland expansion in the African tropics, plus tundra expansion in the forests of modern Eurasia (Wu et al., 2007; Prentice et al., 2011; Binney et al., 2017). These vegetation shifts would have brightened the regional land surface and, barring strong compensating feedbacks, the top of atmosphere. We note that our analysis does not account for other factors outside of moist static energy anomalies that can shift the precipitation centroid zonally. For example, there is evidence for stronger easterly winds across the tropical Atlantic at the LGM (McIntyre & Molfino, 1996; Adkins et al., 2006; McGee et al., 2013; Bradtmiller et al., 2016; Zular et al., 2019) that could shift the maximum vector wind divergence, and thus precipitation centroid, westward, but stronger winds cannot be readily integrated to the energy balance model as an anomalous energy source.

Starting from the ensemble mean mid-Holocene and LGM climates, we simulate the effect of a darker Sahara (mid-Holocene) and a brighter African tropics and Eurasia (LGM) as spatially uniform positive and negative moist static energy anomalies, respectively. This approach carries some important limitations and should be taken as a proof of concept for demonstrating how land surface albedo can modulate the zonal location of the South American precipitation centroid. Our analysis implicitly assumes that the attenuation of the land surface anomaly to the top of atmosphere is spatially uniform, which is unlikely when comparing tropical Africa and Eurasia. This analysis also ignores the role of an apparent shift to a less El Niño-dominant mean climate state after the LGM (Koutavas & Joanides, 2012; Ford et al., 2018), which could affect the zonal energy balance (Boos & Korty, 2016) and was previously argued to contribute to the zonally imbalanced $\delta^{18}O$ signals by decreasing $\delta^{18}O$ everywhere, amplifying the eastern and dampening the western trend (Cheng et al., 2013). However, because this mechanism affects all sites similarly, so it cannot explain the $\Delta\delta^{18}O$ trends that we interpret as changes in the precipitation centroid's location.

4 Results and interpretation

4.1 Isotope gradients and net rainout

The isotope gradients over space are distinct from any one $\delta^{18}O$ record, suggesting there is no single representative site that reflects basin-wide rainout. Figure 3a shows these gradients for the eastern-to-central sites ("eastern domain"; light green) and central-to-western sites ("western domain"; dark green), with the theoretical maximum $\Delta\delta^{18}O$ value of zero labelled as the hydrostat (Chamberlain et al., 2014; Caves et al., 2015; Kukla et al., 2019). The hydrostat is the point where further drying has no affect on $\Delta\delta^{18}O$ because nearly all precipitation is being recycled. The eastern domain gradient is near the hydrostat from the LGM to the early Holocene, then decreases to ∼-2.5‰ in the mid-late Holocene and increases by <1‰ to present. While at the hydrostat, $\Delta\delta^{18}O$ does not capture further drying that likely distinguishes the early-mid Holocene conditions from the mid-late Holocene (P. A. Baker, Seltzer, et al., 2001; Fritz et al., 2004; Cheng et al., 2013; Kukla et al., 2021). The western domain gradient shows a mostly opposing trend, with $\Delta\delta^{18}O$ near ∼-2‰ at the LGM and increasing to zero, the hydrostat, by the mid-Holocene before decreasing to present. The late Holocene $\Delta\delta^{18}O$ value in this domain is similar to the rainfall $\Delta\delta^{18}O$ across the tropical South America today (Salati et al., 1979; Wang et al., 2017). Overall, despite $\delta^{18}O$ shifts that are zonally imbalanced (about twice as large in the eastern and central records compared to the west), the magnitude of $\Delta\delta^{18}O$ change is comparable in each domain, consistent with zonally balanced changes in rainout.

Following previous work using isotope gradients (Salati et al., 1979; Hu et al., 2008; Winnick et al., 2014), we interpret the $\Delta\delta^{18}O$ data as reflecting rainout between two sites and the $\delta^{18}O$ data as recording the net integrated upwind rainout signal. Figure 3b is an attempt to visualize both the local ($\Delta\delta^{18}O$) and upwind ($\delta^{18}O$) rainout signals. Here, the eastern, central, and western $\delta^{18}O$ records are smoothed and plotted together with the space between them colored to illustrate the magnitude of change in $\delta^{18}O$ between each site. This figure shows that the location where $\delta^{18}O$ decreases the most (indicative of the most rainout) shifts from the western domain (dark green) at the LGM to east of the eastern site, over the tropical Atlantic Ocean (blue), by the mid-Holocene, to somewhere in between by the late Holocene.

This interpretive framework explains how the SAPD is zonally balanced despite zonally imbalanced $\delta^{18}O$ records. The western $\delta^{18}O$ shifts are small compared to the eastern record because the focus of rainout is always upwind of the western site. In contrast, the focus of rainout is downwind of the eastern and central sites at the LGM, and upwind of these sites at the mid-Holocene. Put otherwise, the focus of rainout shifts along the moisture trajectory relative to the eastern and central sites, but not the western site, driving larger amplitude $\delta^{18}O$ trends in the eastern and central sites. We note that additional complications at the eastern site, such as competing air-masses (Garreaud et al., 2009; Liu & Battisti, 2015) could modify the relationship between rainout and $\Delta\delta^{18}O$

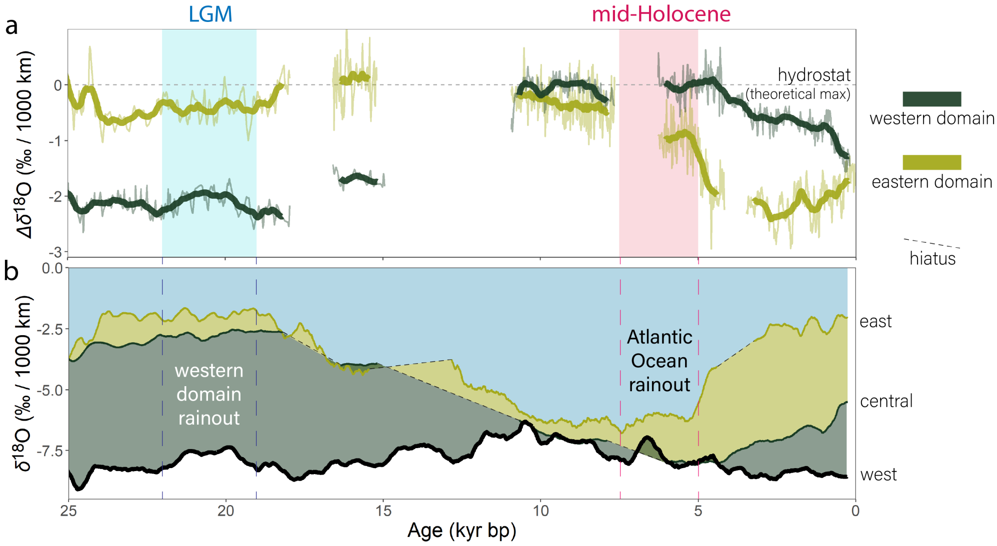

Figure 3. Isotope gradient and individual $\delta^{18}O$ records. (**A**) Eastern-to-central (light green) and central-to-western (dark green) isotopic gradients. More negative $\Delta\delta^{18}O$ is interpreted as more rainout between sites (wetter). (**B**) The three, smoothed $\delta^{18}O$ records (labels on right of panel) (van Breukelen et al., 2008; Cruz et al., 2009; Cheng et al., 2013; Wang et al., 2017). Y-axis color range is proportional to net moisture loss (rainout) within the western (dark green), eastern (light green), or ocean (turquoise) domains. The increase in blue toward the MH reflects a hypothesized increase in rainout over the ocean. Dashed lines with intervals of lighter shading are hiatus periods in the $\delta^{18}O$ records.

through time. We caution against interpreting eastern $\Delta\delta^{18}O$ as quantitative trends in rainout, and we expand on this point in section 5.4.

In addition to the zonally imbalanced $\delta^{18}O$ trends, another enigmatic feature of the $\delta^{18}O$ data is that the records are out-of-phase with one another. The out-of-phase nature of these $\delta^{18}O$ shifts can also be understood in the context of upwind effects. The western $\delta^{18}O$ record decreases from 10-5 ka (Fig. 3b) while $\Delta\delta^{18}O$ stays near the theoretical maximum value of zero (Fig. 3a), consistent with the $\delta^{18}O$ shift being driven by upwind rather than local rainout. Meanwhile, in the last 5 kyr, the focus of decreasing $\delta^{18}O$ shifts inland, first over the eastern domain and next over the western domain, revealing a time-transgressive trend that emerges from the central $\delta^{18}O$ data lagging the eastern record. Thus, the progressive inland migration of the focus of rainout provides a plausible mechanism for the enigmatic lag between these records.

4.2 Reconstructed annual precipitation rates

Our reactive transport results suggest that late Holocene precipitation rates were similar to modern, consistent with similar $\Delta\delta^{18}O$ values between the late Holocene speleothem data and modern rainfall. During the LGM, we find increased rainfall relative to the late Holocene (light blue distribution of Fig. 4a; 3000 $\pm$ 800 mm/yr). This result is consistent with extensive evidence for wetter conditions in western tropical South America (P. A. Baker, Seltzer, et al., 2001; P. A. Baker, Rigsby, et al., 2001; Fritz et al., 2004). When wind speed and transpiration are equal to or greater than modern values (see Methods), calculated rainfall increases to $\sim$3400 $\pm$400 mm/yr to compensate for increased moisture transport and decreased isotopic fractionation associated with transpiration (dark blue distribu-

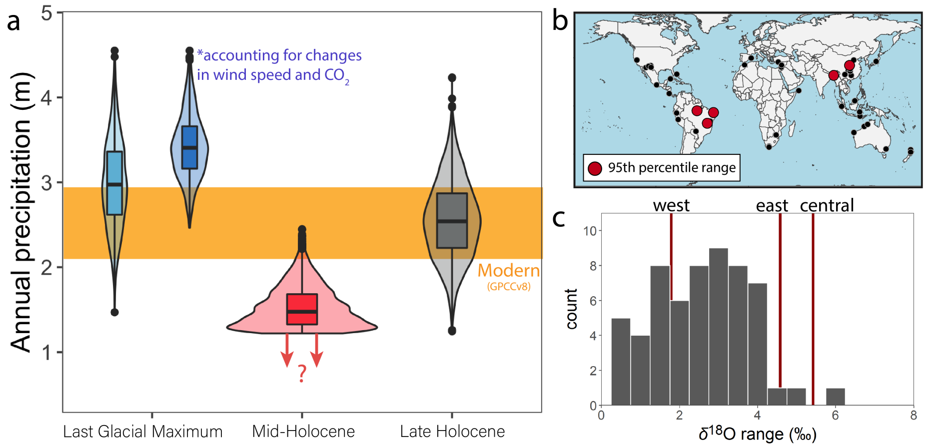

Figure 4. (**A**) Reconstructed precipitation for the LGM (blue), mid-Holocene (red) and late Holocene (gray). Mid-Holocene is restricted at the lower-bound because $\Delta\delta^{18}O$ is at the hydrostat. (**B**) Map of records with $\delta^{18}O$ ranges in the largest 5% (red) and all sites (black). (**C**) The distribution of $\delta^{18}O$ ranges. red, vertical lines show values for the west, central, and western sites discussed in the text. The central and eastern records are in the largest 5 percent of all similar sites (Supplemental text S4).

tions of Fig. 4a). We note that hydrogen isotope composition (δD) of leaf waxes from the Amazon River appears higher at the LGM than before or after, suggesting drier conditions than today (Häggi et al., 2017). However, the signal is small (about 1-2‰ in $\delta^{18}O$) and not inconsistent with our finding that the western domain $\Delta\delta^{18}O$ values are higher at the LGM compared to before and after.

During the mid-Holocene, the reactive transport model simulates rainfall decreasing to ~1200 mm/yr (about half of modern; red distribution of Fig. 4a). As discussed in Kukla et al. (2021), the $\Delta\delta^{18}O$ values in the mid-Holocene straddle zero—the theoretical maximum value for a single moisture trajectory. At this point, further drying has a negligible effect on $\Delta\delta^{18}O$. The shape of the mid-Holocene distribution thus reflects the imposed lower-bound of annual precipitation, effectively restricting the solution to the wettest scenarios.

One limitation to our analysis is that we do not explicitly account for the possibility that changes in the seasonality of rainfall affect one site more than the other. Seasonality could be an issue in northeastern Brazil, where peak precipitation is offset from the central and western sites. However, seasonality, independent of rainout, is unlikely to drive the eastern (or central) $\delta^{18}O$ data because the amplitude of change is equal to or greater than the amplitude of $\delta^{18}O$ seasonality today (see Fig. S4). To formalize this point, we use high and low austral summer insolation results for northeastern Brazil from the isotope-enabled GCM experiments of Liu and Battisti (2015) to show that a 5-8‰ decrease in wet-season precipitation $\delta^{18}O$ is required to explain the low mid-Holocene values (Fig. S8). Changes in monthly precipitation amount have a small effect on annual $\delta^{18}O$, as noted by Liu and Battisti (2015), indicating that a shift in the dominant air-mass cannot explain the speleothem signal. This required decrease in wet-season $\delta^{18}O$ is about four times greater than that simulated by the isotope-enabled GCM (Fig. S8). Given the small influence of precipitation and air-mass changes, it is best explained by an increase in net upwind rainout. We expand on how changes in seasonality and atmospheric circulation affect our conclusions at other sites in the discussion section.

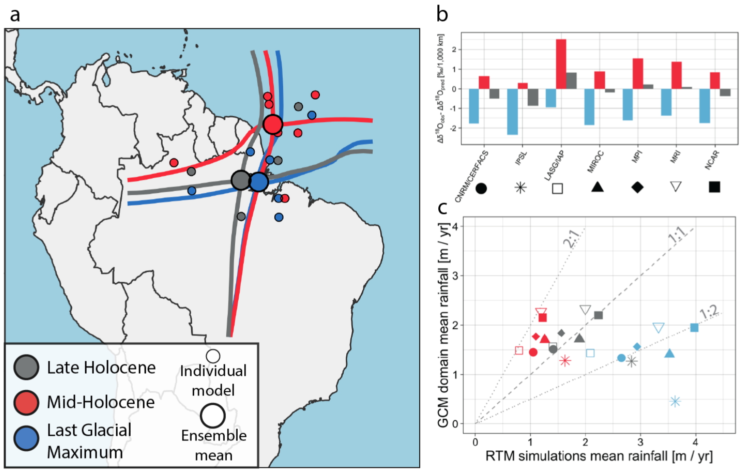

Figure 5. PMIP3/CMIP5 SAM centroid and isotope gradient analysis. (**A**) PMIP3 models show little zonal variation in the tropical South American precipitation centroid from the LGM, mid-Holocene, and late Holocene (pre-industrial) for months NDJFMAM. (**B**) When forced with PMIP3/CMIP5 output, the reactive transport model (Kukla et al., 2019) systematically predicts a steeper-than-observed $\delta^{18}O$ gradient at the mid-Holocene (red bars) and a shallower-than-observed gradient at the LGM (blue bars) with no systematic error in the late Holocene. This result is consistent with the $\delta^{18}O$ error found in the isotope-enabled simulations of Cruz et al. (2009) and Liu and Battisti (2015). (**C**) To match the observed oxygen isotope gradient, the reactive transport model requires similar rainfall amounts as predicted by the PMIP3/CMIP5 models at the late Holocene, but requires drier conditions than PMIP3/CMIP5 at the mid-Holocene and wetter conditions at the LGM.

The reactive transport model estimates of past precipitation show larger SAPD anomalies than predicted by GCMs (Cruz et al., 2009; Liu & Battisti, 2015; Shimizu et al., 2020). GCM simulations of the SAPD have accounted for precession and its impact on land surface heating, but not other "boundary condition" changes such as the land albedo response to vegetation change. If the speleothem $\delta^{18}O$ data reliably reflects past precipitation $\delta^{18}O$, we must consider the possibility that other factors, in addition to (and in response to) precession, shape the late Quaternary SAPD.

Zonal migration of the precipitation centroid should drive larger precipitation anomalies than a zonally static precipitation centroid. Battisti et al. (2014), for example, argues that a zonal shift in the pan-Asian monsoon with changing northern hemisphere summer insolation could explain some of the largest documented speleothem $\delta^{18}O$ shifts. Using the SISALv2 database (Atsawawaranunt et al., 2018; Comas-Bru et al., 2019, 2020) we find that magnitude of $\delta^{18}O$ shifts in the eastern and central records is in the top 5% of all comparable records (duration between 10^3-10^5 years and within 40° of the equator) (see Supplemental text S4) (Fig. 4b, c). The other records with large $\delta^{18}O$ ranges appear near the pan-Asian monsoon region, consistent with these two regions being among the most sensitive to zonal energy anomalies and precipitation shifts (Battisti et al., 2014; Boos & Korty, 2016).

4.3 PMIP3/CMIP5 analysis with energy balance and reactive transport models

Our analyses with the PMIP3/CMIP5 data affirm previous isotope-enabled GCM results (Cruz et al., 2009; Liu & Battisti, 2015). The simulations do not capture zonal migration of the precipitation centroid and they under-estimate the magnitude of $\delta^{18}O$ variation. We find that, while the energy flux equator shifts northward in the mid-Holocene wet season (a result contested by other models; Liu and Battisti (2015); Chiessi et al. (2021)), the energy flux prime meridian does not show any systematic shift to the east or west (Fig. 5a). Meanwhile, when forced with PMIP3/CMIP5 output the reactive transport model correctly predicts late Holocene $\Delta\delta^{18}O$ data, demonstrating that the net rainout in the models is consistent with the isotope data despite broad precipitation biases. During the LGM, however, the PMIP3/CMIP5 output leads to an isotope gradient that is too shallow, consistent with the models being too dry (Fig. 5b,c). In contrast, the simulated isotope gradients are too steep at the mid-Holocene when driven by PMIP3/CMIP5 output, consistent with the models being too wet. Taken together, zonal shifts in the precipitation centroid are negligible in the PMIP3/CMIP5 models and their precipitation anomalies are smaller than suggested by the isotope data, despite good agreement in the late Holocene.

We therefore hypothesize that the the zonal migration of the precipitation centroid can resolve these discrepancies. This hypothesis is outlined in Figure 6, and we address its plausibility in the following subsection. We hypothesize that the precipitation centroid tracks the region of maximum net rainout (decreasing $\delta^{18}O$), located between the central and western records at the Last Glacial Maximum (Fig. 6c, f), upwind of the eastern record at the mid-Holocene (Fig. 6b, e), and somewhere in between in the late Holocene (Fig. 6a, d), consistent with its modern position (Boos & Korty, 2016). While zonal precipitation centroid migration aligns with the $\delta^{18}O$ data and its magnitude of change, it is unclear whether late Quaternary forcings could plausibly drive such zonal shifts.

4.4 Zonal migration of the precipitation centroid in an Energy Balance Model

We find that reasonable zonally asymmetric forcings for the mid-Holocene and LGM, not captured in the PMIP3/CMIP5 models, can cause the precipitation centroid to shift zonally relative to its initial PMIP3/CMIP5 ensemble mean state (Fig. 7). In our energy balance model simulations, the anomalous moist static energy source owed to a darker Sahara at the mid-Holocene is sufficient to pull the energy flux prime meridian east of the eastern speleothem record, consistent with its mid-Holocene $\delta^{18}O$ minimum (Fig. 7d-f). In contrast, a decrease in forest cover in tropical Africa and Eurasia pushes the energy flux prime meridian westward in the LGM (Fig. 7a-c). We note that the location of the energy flux equator-prime meridian intersection approximates, but may be offset from, the location of the precipitation centroid (Boos & Korty, 2016), although this offset should be constant as the precipitation centroid migrates (Adam et al., 2016; Boos & Korty, 2016). The simple energy balance model does not account for changes in the partitioning between latent and sensible heat, but any repartitioning does not alter the total energy flux from the land to the base of the atmospheric column (Laguë et al., 2019). Instead, repartitioning could affect the net energy imbalance via uncertain cloud feedbacks (Laguë et al., 2021) and possibly amplify the imbalance due to latent cooling-driven reductions in outgoing longwave radiation (Boos & Korty, 2016). A decrease in Saharan dustiness would also amplify the energy imbalance, though we do not account for it here. Our analysis shows that the precipitation centroid is sufficiently sensitive to remote forcing to explain the late Quaternary precipitation anomalies, although the exact location of rainout will depend on the initial state (here, from PMIP3/CMIP5) and the relative offset between the energy flux intersection and the precipitation centroid.

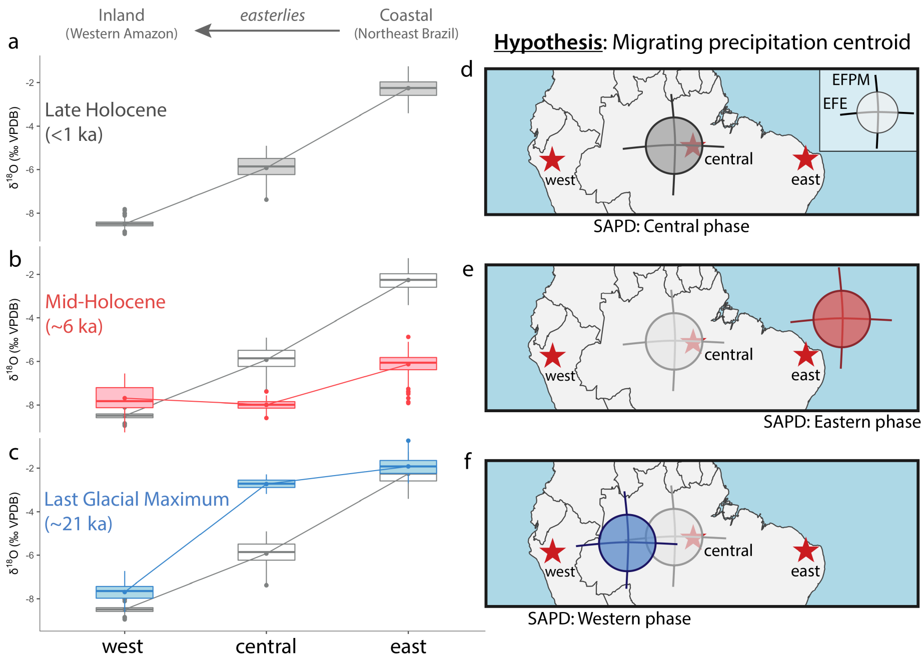

Figure 6. Precipitation centroid migration hypothesis and its isotopic expression. (**A-C**) Show the three distinct isotope profiles of the late Holocene (**A**), mid-Holocene (**B**), and LGM (**C**). Late Holocene is reproduced in panels **B** and **C** for comparison. Lines connect the mean of each site. Data from van Breukelen et al. (2008); Cruz et al. (2009); Cheng et al. (2013); Wang et al. (2017). (**D-F**) Illustrate hypothesized changes in the South American precipitation centroid (intersection of the energy flux equator (EFE) and energy flux prime meridian (EFPM)) based on where most of the $\delta^{18}O$ decrease (rainout) occurs (tropical Atlantic/northeast Brazil at mid-Holocene, and western Amazon at LGM).

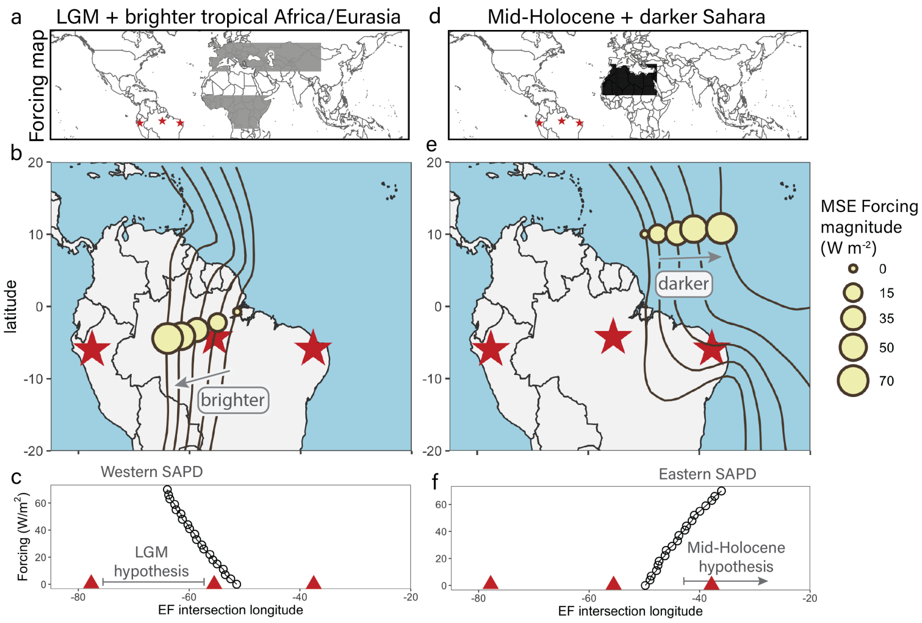

Figure 7. Sensitivity of the SAPD to zonal energy anomalies. Gray and black boxes in the maps of panels (**A**) and (**D**) show the locations of LGM and mid-Holocene moist static energy (MSE) forcings, respectively. Panels (**B**) and (**E**) show the response of the energy flux prime meridian (lines) and energy flux intersection (points; approximating the precipitation centroid) to selected forcing levels for the LGM and mid-Holocene. The energy flux intersection longitude versus the magnitude of forcing is shown in panels (**C**) and (**F**) for the LGM and mid-Holocene. We note that the points on the map panels are not a proposed path of the precipitation centroid in the late Quaternary, but rather the response to different forcing magnitudes starting from the PMIP3/CMIP5 initial conditions.

5 Discussion

5.1 A zonally balanced SAPD

Previous work has argued that the distinct trends between the western and central/eastern $\delta^{18}O$ data reflect either (1) a zonally imbalanced precipitation dipole (Cheng et al., 2013); or (2) changes in the strength of convection, but not the location of peak rainout (Wang et al., 2017). Here, we address how our results support a third scenario—a zonally balanced SAPD that reconciles the zonally imbalanced amplitudes of $\delta^{18}O$ change. We also discuss how accounting for upwind rainout distinguishes our revised $\delta^{18}O$ interpretations from previous work.

Larger $\delta^{18}O$ signals in the eastern and central records do not require larger precipitation anomalies because a shift in the location of peak rainout has a small effect on sites that remain downwind. That is, whether the focus of rainout occurs near the speleothem site or a few hundred kilometers upwind, speleothem $\delta^{18}O$ will be approximately the same as long as the same magnitude of rainout occurs before the airmass reaches that site. We argue that this is why the western $\delta^{18}O$ trends are muted—the focus of rainout remains upwind of the western site for the entirety of the record. This may also explain discrepancies with basin-integrated precipitation isotope data. Häggi et al. (2017), for example, find basin-integrated δD trends that are small ($\sim$1-2‰ in $\delta^{18}O$) and distinct from any one speleothem $\delta^{18}O$ record in the last 50 kyr, consistent with a decoupling of $\delta^{18}O$ and local precipitation amount. The magnitude of total rainout, and basin-integrated precipitation $\delta^{18}O$, appear relatively constant through time, regardless of whether that rainout occurs in the west or east. The western and eastern legs of the SAPD are approximately balanced.

Previous work has applied a different interpretive framework to the central and western $\delta^{18}O$ data to argue that the Amazon was wetter in the mid-Holocene and drier at the LGM, opposing our results (Wang et al., 2017). The key distinction with our work is that Wang et al. (2017) assume that upwind $\delta^{18}O$ is constant (with corrections for temperature and seawater $\delta^{18}O$ following P. A. Baker and Fritz (2015)) such that the central $\delta^{18}O$ record drives all variability in $\Delta\delta^{18}O$. We argue that the assumption of an effectively constant upwind $\delta^{18}O$ value is refuted by data (Cruz et al., 2009)—the strong correlation between central and eastern (upwind) $\delta^{18}O$ records is evidence that upwind $\delta^{18}O$ is propagating downwind without attenuation. Our approach avoids the assumption that upwind moisture loss is constant through time and, as we discuss in the next section, is consistent with evidence that $\delta^{18}O$ is not always strongly coupled with *local* precipitation amount (Wortham et al., 2017; Ward et al., 2019). Within our framework, the wettest time occurs when the isotope gradient is steepest, not when central $\delta^{18}O$ is lowest, consistent with our understanding of how $\Delta\delta^{18}O$ relates to precipitation today (Salati et al., 1979; Pattnayak et al., 2019; Ampuero et al., 2020).

5.2 Zonal and meridional components of precipitation centroid migration

Late Quaternary forcings, including precession and land surface change, should lead to zonal and meridional shifts in the precipitation centroid. The energy flux equator drives north-south migration that is well-documented in late Quaternary proxy records (Arbuszewski et al., 2013; Deplazes et al., 2013; Mulitza et al., 2017; Chiessi et al., 2021), and the energy flux prime meridian drives the east-west component (Boos & Korty, 2016) which we argue is evident in the speleothem $\delta^{18}O$ data. Because the location of the precipitation centroid varies near-linearly with anomalous forcing (rather than abruptly at some threshold; Fig. 7) its spatial migration should cause time-transgressive proxy trends as it reaches different locations at different times. Here, we compare the west-east (LGM to mid-Holocene) and east-west (mid-Holocene to present) SAPD transitions and discuss evidence for zonal and meridional structure of precipitation centroid migration with asynchronous proxy signals, consistent with our hypothesis.

We first focus on a broad comparison of the two SAPD transitions by comparing the eastern-to-central (eastern domain) and central-to-western (western domain) $\Delta\delta^{18}O$ data, shown in Figure 8b. Here, lower values on the y-axis are interpreted as more western domain rainout, and lower values on the x-axis as more eastern domain rainout. If the focus of rainout only migrates zonally, then a west-east trade-off in rainout will mark a diagonal line with slope -1 (as rainout in one domain increases at the expense of the other), and a shift in rainout further east over the ocean will trace a flat line with an intercept near zero (no rainout in the western domain, only moving through the eastern domain) (Fig. 8c, "expected if only zonal"). The $\Delta\delta^{18}O$ data, however, do not follow this trend. Instead, the LGM to early-mid Holocene marks a decrease in western domain rainout (increase in y-axis) with no compensating increase in the east (x-axis remains near zero) (Fig. 8b, points 1-2), followed by a mostly zonal progression into the eastern, then western domain (points 2-3 and 3-4, respectively). The precipitation centroid appears to migrate eastward with a meridional component relative to the speleothem sites from the LGM to early-mid Holocene, and then westward following a zonal pattern through the speleothem sites to present.

This inferred pattern of migration from the $\Delta\delta^{18}O$ data is supported by independent proxy results. In the last eight thousand years, for example, a steeper isotope gradient reflecting more moisture distillation first appears in the eastern domain from ~8-5 ka (points 2-3 of Fig. 8), and next in the western domain from ~5-0 ka (points 3-4) (see also Fig. 3). This result suggests that the precipitation centroid began passing over the central record ~5 thousand years ago, consistent with recent strontium isotope evidence from the same site pointing to high infiltration rates from 6-5 ka with less infiltration before and after (Ward et al., 2019). The timing of migration is also consistent with a shift from dry to wet conditions in a nearby lake (Reis et al., 2017). After ~5 ka, rainfall begins increasing in the western domain and water infiltration rates at the central site temporarily decline (Ward et al., 2019). As discussed earlier, this gradual westward migration of rainout also explains the perplexing lag of central $\delta^{18}O$ behind the eastern record (Fig. 1c, d). The precipitation centroid first reaches the eastern site at ~8-7 ka when $\delta^{18}O$ values are lowest, and later the central site at ~5 ka, in tandem with records of the local water balance (Reis et al., 2017; Ward et al., 2019).

Unlike this east-west migration, the dipole transition from west to east spanning ~20-10 ka does not coincide with a decrease in eastern domain $\Delta\delta^{18}O$, and we suggest this reflects the precipitation centroid moving around, rather than through, the eastern domain (points 1-2 of Fig. 8). Movement around the domain would require a meridional component of precipitation centroid migration reflected by a change in $\Delta\delta^{18}O$ in one domain that is not balanced by a corresponding change in the other (Fig. 8c, bottom panel). It is possible that the precipitation centroid moved southeast around the central $\delta^{18}O$ site as there is evidence for wetter conditions to the southeast (Whitney et al., 2011; Fornace et al., 2016) and drier conditions to the north (Deplazes et al., 2013; Zular et al., 2019), as well as some evidence for a south-shift of the energy flux equator (Arbuszewski et al., 2013). The southeast appears to become drier around 12 ka, approximately when a nearby speleothem $\delta^{18}O$ shift occurs that is consistent with decreased Amazon and more Atlantic-derived moisture (Fig. S9) (Novello et al., 2017, 2018).

As the precipitation centroid migrates further east, after ~12 ka, pollen data from semi-arid northeastern Brazil (near the eastern $\delta^{18}O$ site) suggest humid conditions from ~10.9-6.7 ka (De Oliveira et al., 1999). Humidity peaks halfway through this interval (~8.9 ka) when eastern $\delta^{18}O$ reaches its lowest values (De Oliveira et al., 1999; Cruz et al., 2009), suggesting this marks the easternmost extent and turning point of the precipitation centroid. As discussed earlier, this timing also corresponds with the onset of the time-transgressive westward shift in wet conditions that continues to the present. While

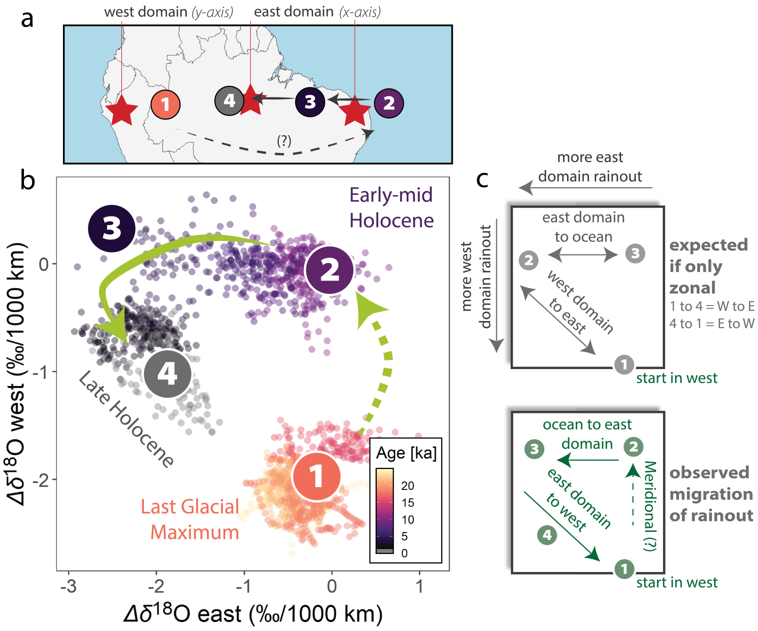

Figure 8. Isotope gradients reflect zonal and meridional shifts in the precipitation centroid. (**A**) Map of speleothem sites showing the east and west domains—the axes of panel B—and a schematic for the interpretation of panel B. (**B**) Crossplot of eastern and western domain data (derived from data in van Breukelen et al. (2008); Cruz et al. (2009); Cheng et al. (2013); Wang et al. (2017)). Numbered points in B correspond with numbers in panels A and C. (**C**) More negative $\Delta\delta^{18}O$ refers to more rainout in a given domain. Data should track a sideways "V" shape if the focus of rainout migrates only zonally (top panel, note different order of numbers). However, the LGM to early-mid Holocene does not follow this zonal trajectory, suggesting a meridional component (dashed arrow).

more work is needed to trace the past focus of rainfall, we suggest the progressive shifts in wet conditions across the continent (both east-west and west-east) provide empirical support and a testable framework for the pattern of precipitation centroid migration.

5.3 Mechanisms for zonal precipitation centroid migration

While climate model simulations are necessary to assess the dynamical drivers of precipitation centroid migration, our analysis allows us to present testable hypotheses. For example, the greening of the Sahara at the mid-Holocene (about 70 W/m^2 anomalous heat source at top of atmosphere; Boos and Korty (2016)) is likely sufficient to drive the energy flux prime meridian eastward entirely over the tropical Atlantic (Fig. 7e, f). Comparison to proxy records from Africa generally support this remote influence on tropical South American rainfall. Dust flux records of West African Monsoon behavior show pronounced precession-scale variability in the last 240 kyr with prominent exceptions at $\sim$30, $\sim$70, and $\sim$150 ka when dust fluxes "skip" precession beats (Skonieczny et al., 2019). In South America, western Amazon $\delta^{18}O$ records lose sensitivity to precession at the same times (and $\Delta\delta^{18}O$ where there is data, in the $\sim$30 ka case; Fig. S10) (Mosblech et al., 2012; Cheng et al., 2013; Wang et al., 2017). Further, there is a rapid increase in $\delta^{18}O$ at the eastern site at $\sim$5 ka, consistent with a westward (inland) shift of rainout, contemporaneous with the termination of the African Humid Period in North Africa (Shanahan et al., 2015) where increasing land albedo would provide an anomalous energy sink. These similarities are mostly preliminary and more data is needed to test if they hold over space and time, but they are consistent with expectations if the zonal location of the precipitation centroid was sensitive to Saharan albedo.

At the LGM, vegetation change that increases land albedo in tropical Africa and Eurasia could push the energy flux prime meridian westward. However, it is not clear if the magnitude of forcing required for this shift could be accomplished by the LGM vegetation change alone. For example, low $\Delta\delta^{18}O$ values (along with high runoff (Nace et al., 2014)) are a persistent feature in the western domain for at least $\sim$20 kyr before the LGM (Fig. S10), suggesting the cause of a westward shift in rainout is not unique to this time interval. African dust fluxes were persistently high from 40-20 ka, consistent with a remote albedo forcing, but data for other possible drivers of precipitation centroid migration, such as the strength of the easterlies, is sparse at this time.

Based on the zonal, meridional, and hysteresis-like migration of the South American precipitation centroid, we suggest that multiple forcing mechanisms operate at different times to drive these complex, precession-scale patterns. Remote land albedo change could play a particularly important role in driving zonal shifts in rainout, but more sophisticated climate model simulations are needed to rigorously test these hypotheses. We note that Heinrich and Dansgaard/Oeschger events are also linked to remote forcing of tropical South American precipitation (Arz et al., 1998; Nace et al., 2014; Kanner et al., 2012), but these shorter, millennial-scale events are beyond the scope of this study.

5.4 Air-mass and seasonality complications

Up to now, our interpretation of a zonal shift in the precipitation centroid has hinged on the assumption that the three speleothem sites are isotopically connected through time. Here, we discuss how relaxing this assumption does not necessarily invalidate our conclusions. This assumption warrants scrutiny because, at least in the eastern-to-central record domain, the timing of peak precipitation and the relevant air-mass can differ between sites (Fig. S4; Garreaud et al. (2009); Liu and Battisti (2015)) suggesting the isotopic connection may not be strong through time.

For simplicity, we consider two forms of isotopic connectivity between sites: (1) an 'air-mass connection', where the same air mass rains out at both sites; and (2) a 'recycling connection' where rainout at one site evaporates and re-precipitates at the other. An air-mass connection implies a recycling connection and allows upwind isotopic signals to propagate fully downwind. When two sites share only a recycling connection, each site is dominated by a different air-mass and the upwind signal propagates downwind with some attenuation due to air-mass mixing. While changes in circulation might alter the strength of the air-mass connection across tropical South America through time, the recycling connection is likely more robust. For example, about half of western Amazon rainfall is derived from upwind recycling (Zemp et al., 2017; Staal et al., 2018) and upwind (northeastern Brazil) transpiration can travel over 1000 km before re-precipitating out, connecting the east and west (Staal et al., 2018).

First, we note that if two sites share an air-mass and recycling connection, then the mean isotope gradient is insensitive to differences in the timing of peak precipitation between them. We demonstrate this point with a toy model that simulates the isotope gradient between two sites that have different phases of precipitation seasonality (Supplemental Text S5). Differences in the seasonal phase lead to $\Delta\delta^{18}O$ errors (relative to the in-phase case), but these errors are negligible—less than 1% of the seasonal $\Delta\delta^{18}O$ amplitude (Figs. S11 and S12). Thus, a difference in the timing of peak precipitation—as between the eastern and central sites—does not, itself, invalidate the $\Delta\delta^{18}O$ framework.

Still, our conclusions could be impacted if the air-mass connection between sites is weak at some point in time. We evaluate two additional additional scenarios that address this possibility. First, we assume there is a weak air-mass connection between the eastern and central sites. In this case, the high-$\delta^{18}O$ values at these sites during the LGM indicate that their air-masses are delivering undistilled moisture. The precipitation centroid—where moisture distillation is strongest—is likely situated to the west. Toward the mid-Holocene, eastern and central $\delta^{18}O$ decrease in tandem, with no evidence for the downwind attenuation that is expected if upwind recycling was mixing with an independent air-mass. Perhaps $\delta^{18}O$ of the central site's air-mass also decreased from the LGM to mid-Holocene, hiding the attenuation. In this case, lest we invoke a third air-mass somehow, the central signal should propagate west. Wang et al. (2017) explain the lack of western signal by invoking an increase in plant transpiration, but this mechanism has been discredited (Pattnayak et al., 2019; Ampuero et al., 2020).

In the alternate scenario, we assume the eastern and central sites share an air-mass connection with each other, but not the western site. In this case, the eastern and central $\delta^{18}O$ shift from the LGM to mid-Holocene makes sense, however it is not consistent with the lack of a signal in the west. The signal could be masked by a coincident decrease in the western air-mass's rainout, but such a decrease may also be related to a zonal shift in the precipitation centroid. Still, western $\delta^{18}O$ shifts directions to track the central site as soon as $\Delta\delta^{18}O$ reaches the theoretical maximum value for two sites with a strong air-mass connection. Without a strong air-mass connection, this western $\delta^{18}O$ shift and the central and eastern $\delta^{18}O$ decrease after the LGM must be somewhat coincidental, driven by coeval changes in independent air-masses that happen to cancel out the attenuation of the upwind signal while obeying the theoretical maximum $\Delta\delta^{18}O$ of a single air-mass system. Arguments against a strong air-mass connection should address how these apparently unattenuated signals occur in the speleothem data. Overall, we argue that uncertainty in the strength of the air-mass connection makes our quantitative precipitation reconstruction less certain, but it does not conflict with our zonal precipitation centroid migration hypothesis.

6 Conclusion

Our analysis provides a path forward for resolving the enigmatic, non-uniform trends in tropical South American speleothem $\delta^{18}O$, but it rests on assumptions, many previously discussed, that deserve further scrutiny. One critical assumption that is difficult to address is that speleothem $\delta^{18}O$ reliably tracks precipitation $\delta^{18}O$ at all sites. Kinetic fractionation and other confounding processes could decouple speleothem and precipitation $\delta^{18}O$, challenging our model approach. Such effects have not been documented in these speleothems (van Breukelen et al., 2008; Cruz et al., 2009; Cheng et al., 2013; Wang et al., 2017), but additional proxy constraints (such as triple oxygen and mass-48 clumped isotopes) will provide more rigorous tests of local and kinetic effects (Huth et al., 2022). Another limitation lies in the simplified energy balance modeling approach. The goal of these model exercises is to present plausible drivers of zonal rainout shifts for further testing, while recognizing that our list of drivers is not exhaustive. Future studies of the SAPD with more sophisticated models should analyze the zonal location of the energy flux prime meridian and its relation to zonal precipitation patterns to test whether this zonal precipitation centroid migration effect is present.

It is also fair to question whether the discrepancies between proxies and isotope-enabled GCMs are resolvable, as we posit. GCMs are known to struggle with tropical South American precipitation—there is substantial inter-model spread and dry-bias in seasonal and annual rainfall that complicate their application to exotic, paleoclimate states (Li et al., 2006; Ribas et al., 2022). However, these models show better agreement in their simulated precipitation change, and their precipitation biases do not appear to cause biases in net rainout (see Fig. 5c). We also reiterate that, while we question whether precession without land albedo change sufficiently explains the late Quaternary SAPD, our work should not be taken to discredit the role of precession more generally. We expect that the spatial pattern and amplitude of $\delta^{18}O$ anomalies can vary from one precession cycle to the next, depending on how orbital forcing interacts with other forcings and feedbacks within the Earth system. A zonal shift in the precipitation centroid is not required to explain zonally opposing precipitation anomalies, but it helps explain certain features of the late Quaternary proxy data, including the zonally imbalanced amplitude of $\delta^{18}O$ change and their notable phase-shifted trends. Our results build on previous work (Battisti et al., 2014) suggesting that zonal forcings may help explain some of the enigmatic proxy records found in places where tropical precipitation is energetically primed to migrate east-west.

Data Availability Statement

Code and data associated with this study can be found through Zenodo (Kukla et al., 2022) and Github (`https://github.com/tykukla/ZonalPrecipPatterns-Amazon`). The Zenodo/Github repository includes code and results for the energy balance and reactive transport model analysis, SISALv2 analysis, speleothem $\delta^{18}O$ data cleaning and smoothing, and the proxy compilation in Figure 1 of the main text. We note that the Tigre Perdido record (van Breukelen et al., 2008) from the western composite data was downloaded from the SISAL database (siteID: 25), while other speleothem records were provided by the original authors or taken from the supplementary materials of the relevant publication.

Acknowledgments

We thank F. W. Cruz, J. K. C. Rugenstein, W. Boos, and C. Skinner for thoughtful discussion, as well as Paul Baker and two anonymous reviewers whose comments significantly improved the manuscript. We also thank F. W. Cruz, X. Wang, and H. Cheng for sharing the speleothem data used in this study. We thank S. J. Burns for helpful comments on an earlier version of this manuscript. We acknowledge the SISAL (Speleothem Isotopes Synthesis and Analysis) working group and data contributors. SISAL is a working group of the Past Global Changes (PAGES) programme. We acknowledge the World Climate Research Programme's Working Group on Coupled Modelling, which is responsible for CMIP, and we thank the climate modeling groups for producing and making available their model output. For CMIP the U.S. Department of Energy's Program for Climate Model Diagnosis and Intercomparison provides coordinating support and led development of software infrastructure in partnership with the Global Organization for Earth System Science Portals. We thank developers and providers of all data sources used in this study including GPCCv8, NCEP Reanalysis 2, GNIP, and PMIP3/CMIP5. NCEP_Reanalysis 2 data provided by the NOAA/OAR/ESRL PSD, Boulder, Colorado, USA from their web site at https://www.esrl.noaa.gov/psd. T. K. acknowledges support from the Stanford McGee/Levorsen research grant. This research was supported by the NOAA Climate and Global Change Postdoctoral Fellowship Program, administered by UCAR's Cooperative Programs for the Advancement of Earth System Science (CPAESS) under the NOAA Science Collaboration Program award #NA21OAR4310383. The authors declare no competing interests.

References

Abouchami, W., & Zabel, M. (2003, August). Climate forcing of the Pb isotope record of terrigenous input into the Equatorial Atlantic. *Earth and Planetary Science Letters*, *213*(3-4), 221–234. doi: 10.1016/S0012-821X(03)00304-2

Adam, O., Bischoff, T., & Schneider, T. (2016, October). Seasonal and Interannual Variations of the Energy Flux Equator and ITCZ. Part II: Zonally

Varying Shifts of the ITCZ. *Journal of Climate*, *29*(20), 7281–7293. doi: 10.1175/JCLI-D-15-0710.1

Adkins, J., deMenocal, P., & Eshel, G. (2006, December). The "African humid period" and the record of marine upwelling from excess ^{230} Th in Ocean Drilling Program Hole 658C. *Paleoceanography*, *21*(4), PA4203. doi: 10.1029/2005PA001200

Ampuero, A., Stríkis, N. M., Apaéstegui, J., Vuille, M., Novello, V. F., Espinoza, J. C., ... Sifeddine, A. (2020, February). The Forest Effects on the Isotopic Composition of Rainfall in the Northwestern Amazon Basin. *Journal of Geophysical Research: Atmospheres*, *125*(4). doi: 10.1029/2019JD031445

Arbuszewski, J. A., deMenocal, P. B., Cléroux, C., Bradtmiller, L., & Mix, A. (2013, November). Meridional shifts of the Atlantic intertropical convergence zone since the Last Glacial Maximum. *Nature Geoscience*, *6*(11), 959–962. doi: 10.1038/ngeo1961

Arz, H. W., Pätzold, J., & Wefer, G. (1998). Correlated Millennial-Scale Changes in Surface Hydrography and Terrigenous Sediment Yield Inferred from Last-Glacial Marine Deposits off Northeastern Brazil. *Quaternary Research*, *50*, 157–166.

Atsawawaranunt, K., Comas-Bru, L., Mozhdehi, S. A., Deininger, M., Harrison, S. P., Baker, A., ... Scroxton, N. (2018). The SISAL database: A global resource to document oxygen and carbon isotope records from speleothems. *Earth System Science Data*, *10*, 1687–1713.

Baker, J. C. A., Gloor, M., Spracklen, D. V., Arnold, S. R., Tindall, J. C., Clerici, S. J., ... Brienen, R. J. W. (2016, November). What drives interannual variation in tree ring oxygen isotopes in the Amazon?: WHAT DRIVES AMAZON TREE RING δ ^{18} O? *Geophysical Research Letters*, *43*(22), 11,831–11,840. doi: 10.1002/2016GL071507

Baker, P. A., & Fritz, S. C. (2015, September). Nature and causes of Quaternary climate variation of tropical South America. *Quaternary Science Reviews*, *124*, 31–47. doi: 10.1016/j.quascirev.2015.06.011

Baker, P. A., Rigsby, C. A., Seltzer, G. O., Fritz, S. C., Lowenstein, T. K., Bacher, N. P., & Veliz, C. (2001, February). Tropical climate changes at millennial and orbital timescales on the Bolivian Altiplano. *Nature*, *409*(6821), 698–701. doi: 10.1038/35055524

Baker, P. A., Seltzer, G. O., Fritz, S. C., Dunbar, R. B., Grove, M. J., Tapia, P. M., ... Broda, J. P. (2001, January). The History of South American Tropical Precipitation for the Past 25,000 Years. *Science*, *291*(5504), 640–643. doi: 10.1126/science.291.5504.640

Battisti, D. S., Ding, Q., & Roe, G. H. (2014, November). Coherent pan-Asian climatic and isotopic response to orbital forcing of tropical insolation. *Journal of Geophysical Research: Atmospheres*, *119*(21), 11,997–12,020. doi: 10.1002/2014JD021960

Binney, H., Edwards, M., Macias-Fauria, M., Lozhkin, A., Anderson, P., Kaplan, J. O., ... Zernitskaya, V. (2017, February). Vegetation of Eurasia from the last glacial maximum to present: Key biogeographic patterns. *Quaternary Science Reviews*, *157*, 80–97. doi: 10.1016/j.quascirev.2016.11.022

Boers, N., Rheinwalt, A., Bookhagen, B., Barbosa, H. M. J., Marwan, N., Marengo, J., & Kurths, J. (2014, October). The South American rainfall dipole: A complex network analysis of extreme events: BOERS ET AL. *Geophysical Research Letters*, *41*(20), 7397–7405. doi: 10.1002/2014GL061829

Boos, W. R., & Korty, R. L. (2016, December). Regional energy budget control of the intertropical convergence zone and application to mid-Holocene rainfall. *Nature Geoscience*, *9*(12), 892–897. doi: 10.1038/ngeo2833

Braconnot, P., Harrison, S. P., Kageyama, M., Bartlein, P. J., Masson-Delmotte, V., Abe-Ouchi, A., ... Zhao, Y. (2012, June). Evaluation of climate models using palaeoclimatic data. *Nature Climate Change*, *2*(6), 417–424. doi: 10.1038/nclimate1456

Bradtmiller, L. I., McGee, D., Awalt, M., Evers, J., Yerxa, H., Kinsley, C. W., & deMenocal, P. B. (2016, January). Changes in biological productivity along the northwest African margin over the past 20,000 years. *Paleoceanography*, *31*(1), 185–202. doi: 10.1002/2015PA002862

Brienen, R. J. W., Helle, G., Pons, T. L., Guyot, J.-l., & Gloor, M. (2012). Oxygen isotopes in tree rings are a good proxy for Amazon precipitation and El Niño-Southern Oscillation variability. *Proceedings of the National Academy of Sciences*, *109*(42). doi: 10.1073/pnas.1205977109

Campos, J. L. P. S., Cruz, F. W., Ambrizzi, T., Deininger, M., Vuille, M., Novello, V. F., & Strikis, N. M. (2019, July). Coherent South American Monsoon Variability During the Last Millennium Revealed Through High-Resolution Proxy Records. *Geophysical Research Letters*, *46*(14), 8261–8270. doi: 10.1029/2019GL082513

Campos, M. C., Chiessi, C. M., Novello, V. F., Crivellari, S., Campos, J. L. P. S., Albuquerque, A. L. S., … Mendes, V. R. (2022, December). South American precipitation dipole forced by interhemispheric temperature gradient. *Scientific Reports*, *12*(1), 10527. doi: 10.1038/s41598-022-14495-1

Caves, J. K., Winnick, M. J., Graham, S. A., Sjostrom, D. J., Mulch, A., & Chamberlain, C. P. (2015). Role of the westerlies in Central Asia climate over the Cenozoic. *Earth and Planetary Science Letters*, *428*, 33–43. doi: 10.1016/j.epsl.2015.07.023

Chamberlain, C. P., Winnick, M. J., Mix, H. T., Chamberlain, S. D., & Maher, K. (2014). The impact of neogene grassland expansion and aridification on the isotopic composition of continental precipitation. *Global Biogeochemical Cycles*, *28*(9), 992–1004. doi: 10.1002/2014GB004822

Cheng, H., Sinha, A., Cruz, F. W., Wang, X., Edwards, R. L., D'Horta, F. M., … Auler, A. S. (2013). Climate change patterns in Amazonia and biodiversity. *Nature Communications*, *4*, 1–6. doi: 10.1038/ncomms2415

Chiessi, C. M., Mulitza, S., Taniguchi, N. K., Prange, M., Campos, M. C., Häggi, C., … Cruz, F. W. (2021, April). Mid- to Late Holocene Contraction of the Intertropical Convergence Zone Over Northeastern South America. *Paleoceanography and Paleoclimatology*, *36*(4). doi: 10.1029/2020PA003936

Comas-Bru, L., Harrison, S. P., Werner, M., Rehfeld, K., Scroxton, N., Veiga-Pires, C., & SISAL working group members. (2019, August). Evaluating model outputs using integrated global speleothem records of climate change since the last glacial. *Climate of the Past*, *15*(4), 1557–1579. doi: 10.5194/cp-15-1557-2019

Comas-Bru, L., Rehfeld, K., Roesch, C., Amirnezhad-Mozhdehi, S., Harrison, S. P., Atsawawaranunt, K., … SISAL Working Group members (2020, October). SISALv2: A comprehensive speleothem isotope database with multiple age–depth models. *Earth System Science Data*, *12*(4), 2579–2606. doi: 10.5194/essd-12-2579-2020

Cruz, F. W., Vuille, M., Burns, S. J., Wang, X., Cheng, H., Werner, M., … Nguyen, H. (2009, March). Orbitally driven east–west antiphasing of South American precipitation. *Nature Geoscience*, *2*(3), 210–214. doi: 10.1038/ngeo444

Dee, S., Noone, D., Buenning, N., Emile-Geay, J., & Zhou, Y. (2015, January). SPEEDY-IER: A fast atmospheric GCM with water isotope physics. *Journal of Geophysical Research: Atmospheres*, *120*(1), 73–91. doi: 10.1002/2014JD022194

De Oliveira, P. E., Barreto, A. M. F., & Suguio, K. (1999, September). Late Pleistocene/Holocene climatic and vegetational history of the Brazilian caatinga: The fossil dunes of the middle São Francisco River. *Palaeogeography, Palaeoclimatology, Palaeoecology*, *152*(3-4), 319–337. doi:

10.1016/S0031-0182(99)00061-9
Deplazes, G., Lückge, A., Peterson, L. C., Timmermann, A., Hamann, Y., Hughen, K. A., ... Haug, G. H. (2013, March). Links between tropical rainfall and North Atlantic climate during the last glacial period. *Nature Geoscience*, *6*(3), 213–217. doi: 10.1038/ngeo1712
Ford, H. L., McChesney, C. L., Hertzberg, J. E., & McManus, J. F. (2018, November). A Deep Eastern Equatorial Pacific Thermocline During the Last Glacial Maximum. *Geophysical Research Letters*, *45*(21). doi: 10.1029/2018GL079710
Fornace, K. L., Whitney, B. S., Galy, V., Hughen, K. A., & Mayle, F. E. (2016, March). Late Quaternary environmental change in the interior South American tropics: New insight from leaf wax stable isotopes. *Earth and Planetary Science Letters*, *438*, 75–85. doi: 10.1016/j.epsl.2016.01.007
Fritz, S. C., Baker, P. A., Lowenstein, T. K., Seltzer, G. O., Rigsby, C. A., Dwyer, G. S., ... Luo, S. (2004, January). Hydrologic variation during the last 170,000 years in the southern hemisphere tropics of South America. *Quaternary Research*, *61*(01), 95–104. doi: 10.1016/j.yqres.2003.08.007
Garreaud, R. D., Vuille, M., Compagnucci, R., & Marengo, J. (2009, October). Present-day South American climate. *Palaeogeography, Palaeoclimatology, Palaeoecology*, *281*(3-4), 180–195. doi: 10.1016/j.palaeo.2007.10.032
Gat, J. R., & Matsui, E. (1991). Atmospheric water balance in the Amazon basin: An isotopic evapotranspiration model. *Journal of Geophysical Research*, *96*(D7), 13179. doi: 10.1029/91JD00054
Grootes, P. M., Stuiver, M., Thompson, L. G., & Mosley-Thompson, E. (1989). Oxygen isotope changes in tropical ice, Quelccaya, Peru. *Journal of Geophysical Research*, *94*(D1), 1187. doi: 10.1029/JD094iD01p01187
Häggi, C., Chiessi, C. M., Merkel, U., Mulitza, S., Prange, M., Schulz, M., & Schefuß, E. (2017, December). Response of the Amazon rainforest to late Pleistocene climate variability. *Earth and Planetary Science Letters*, *479*, 50–59. doi: 10.1016/j.epsl.2017.09.013
Haug, G. H. (2001, August). Southward Migration of the Intertropical Convergence Zone Through the Holocene. *Science*, *293*(5533), 1304–1308. doi: 10.1126/science.1059725
Hu, C., Henderson, G. M., Huang, J., Xie, S., Sun, Y., & Johnson, K. R. (2008, February). Quantification of Holocene Asian monsoon rainfall from spatially separated cave records. *Earth and Planetary Science Letters*, *266*(3-4), 221–232. doi: 10.1016/j.epsl.2007.10.015
Huth, T. E., Passey, B. H., Cole, J. E., Lachniet, M. S., McGee, D., Denniston, R. F., ... Levin, N. E. (2022, February). A framework for triple oxygen isotopes in speleothem paleoclimatology. *Geochimica et Cosmochimica Acta*, *319*, 191–219. doi: 10.1016/j.gca.2021.11.002
Kanner, L. C., Burns, S. J., Cheng, H., & Edwards, R. L. (2012, February). High-Latitude Forcing of the South American Summer Monsoon During the Last Glacial. *Science*, *335*(6068), 570–573. doi: 10.1126/science.1213397
Keys, P. W., van der Ent, R. J., Gordon, L. J., Hoff, H., Nikoli, R., & Savenije, H. H. G. (2012, February). Analyzing precipitationsheds to understand the vulnerability of rainfall dependent regions. *Biogeosciences*, *9*(2), 733–746. doi: 10.5194/bg-9-733-2012
Konecky, B. L., Noone, D. C., & Cobb, K. M. (2019, February). The Influence of Competing Hydroclimate Processes on Stable Isotope Ratios in Tropical Rainfall. *Geophysical Research Letters*, *46*(3), 1622–1633. doi: 10.1029/2018GL080188
Koutavas, A., & Joanides, S. (2012, December). El Niño-Southern Oscillation extrema in the Holocene and Last Glacial Maximum: ENSO EXTREMA IN THE HOLOCENE AND LGM. *Paleoceanography*, *27*(4). doi:

10.1029/2012PA002378

Kukla, T., Ahlström, A., Maezumi, S. Y., Chevalier, M., Lu, Z., Winnick, M. J., & Chamberlain, C. P. (2021, July). The resilience of Amazon tree cover to past and present drying. *Global and Planetary Change*, *202*, 103520. doi: 10.1016/j.gloplacha.2021.103520

Kukla, T., Winnick, M. J., Laguë, M. M., & Xia, Z. (2022). Project files, data, and code. *Zenodo*. doi: 10.5281/zenodo.7495709

Kukla, T., Winnick, M. J., Maher, K., Ibarra, D. E., & Chamberlain, C. P. (2019, January). The Sensitivity of Terrestrial δ [18] O Gradients to Hydroclimate Evolution. *Journal of Geophysical Research: Atmospheres*, *124*, 563–582. doi: 10.1029/2018JD029571

Laguë, M. M., Bonan, G. B., & Swann, A. L. S. (2019). Separating the Impact of Individual Land Surface Properties on the Terrestrial Surface Energy Budget in both the Coupled and Uncoupled Land–Atmosphere System. *Journal of Climate*, *32*, 20.

Laguë, M. M., Swann, A. L. S., & Boos, W. R. (2021, May). Radiative feedbacks on land surface change and associated tropical precipitation shifts. *Journal of Climate*, 1–63. doi: 10.1175/JCLI-D-20-0883.1

Lee, J.-E., Johnson, K., & Fung, I. (2009). Precipitation over South America during the Last Glacial Maximum: An analysis of the "amount effect" with a water isotope-enabled general circulation model. *Geophysical Research Letters*, *36*(19), L19701. doi: 10.1029/2009GL039265

Li, W., Fu, R., & Dickinson, R. E. (2006). Rainfall and its seasonality over the Amazon in the 21st century as assessed by the coupled models for the IPCC AR4. *Journal of Geophysical Research*, *111*(D2). doi: 10.1029/2005JD006355

Liu, X., & Battisti, D. S. (2015, June). The Influence of Orbital Forcing of Tropical Insolation on the Climate and Isotopic Composition of Precipitation in South America. *Journal of Climate*, *28*(12), 4841–4862. doi: 10.1175/JCLI-D-14-00639.1

Lu, Z., Zhang, Q., Miller, P. A., Zhang, Q., Berntell, E., & Smith, B. (2021, January). Impacts of Large-Scale Sahara Solar Farms on Global Climate and Vegetation Cover. *Geophysical Research Letters*, *48*(2). doi: 10.1029/2020GL090789

Martin, L., Bertaux, J., Corrège, T., Ledru, M.-P., Mourguiart, P., Sifeddine, A., … Turcq, B. (1997, January). Astronomical Forcing of Contrasting Rainfall Changes in Tropical South America between 12,400 and 8800 cal yr B.P. *Quaternary Research*, *47*(1), 117–122. doi: 10.1006/qres.1996.1866

Mason, C. C., Romans, B. W., Stockli, D. F., Mapes, R. W., & Fildani, A. (2019, June). Detrital zircons reveal sea-level and hydroclimate controls on Amazon River to deep-sea fan sediment transfer. *Geology*, *47*(6), 563–567. doi: 10.1130/G45852.1

McGee, D., deMenocal, P., Winckler, G., Stuut, J., & Bradtmiller, L. (2013, June). The magnitude, timing and abruptness of changes in North African dust deposition over the last 20,000yr. *Earth and Planetary Science Letters*, *371–372*, 163–176. doi: 10.1016/j.epsl.2013.03.054

McIntyre, A., & Molfino, B. (1996, December). Forcing of Atlantic Equatorial and Subpolar Millennial Cycles by Precession. *Science*, *274*(5294), 1867–1870. doi: 10.1126/science.274.5294.1867

Mosblech, N. A. S., Bush, M. B., Gosling, W. D., Hodell, D., Thomas, L., van Calsteren, P., … van Woesik, R. (2012, November). North Atlantic forcing of Amazonian precipitation during the last ice age. *Nature Geoscience*, *5*(11), 817–820. doi: 10.1038/ngeo1588

Mulitza, S., Chiessi, C. M., Schefuß, E., Lippold, J., Wichmann, D., Antz, B., … Zhang, Y. (2017, June). Synchronous and proportional deglacial changes in Atlantic meridional overturning and northeast Brazilian precipitation: AMOC and Precipitation over NE Brazil. *Paleoceanography*, *32*(6), 622–633. doi: 10.1002/2017PA003084

Nace, T. E., Baker, P. A., Dwyer, G. S., Silva, C. G., Rigsby, C. A., Burns, S. J., ... Zhu, J. (2014, December). The role of North Brazil Current transport in the paleoclimate of the Brazilian Nordeste margin and paleoceanography of the western tropical Atlantic during the late Quaternary. *Palaeogeography, Palaeoclimatology, Palaeoecology*, *415*, 3–13. doi: 10.1016/j.palaeo.2014.05.030

Nogués-Paegle, J., & Mo, K. C. (1997, February). Alternating Wet and Dry Conditions over South America during Summer. *Monthly Weather Review*, *125*(2), 279–291. doi: 10.1175/1520-0493(1997)125⟨0279:AWADCO⟩2.0.CO;2

Novello, V. F., Cruz, F. W., Moquet, J. S., Vuille, M., de Paula, M. S., Nunes, D., ... Campos, J. L. P. S. (2018, May). Two Millennia of South Atlantic Convergence Zone Variability Reconstructed From Isotopic Proxies. *Geophysical Research Letters*, *45*(10), 5045–5051. doi: 10.1029/2017GL076838

Novello, V. F., Cruz, F. W., Vuille, M., Stríkis, N. M., Edwards, R. L., Cheng, H., ... Santos, R. V. (2017, December). A high-resolution history of the South American Monsoon from Last Glacial Maximum to the Holocene. *Scientific Reports*, *7*(1). doi: 10.1038/srep44267

Pattnayak, K., Tindall, J., Brienen, R., Barichivich, J., & Gloor, E. (2019, October). Can we detect changes in Amazon forest structure using measurements of the isotopic composition of precipitation? *Geophysical Research Letters*, *46*. doi: 10.1029/2019GL084749

Prado, L. F., Wainer, I., & Chiessi, C. M. (2013, December). Mid-Holocene PMIP3/CMIP5 model results: Intercomparison for the South American Monsoon System. *The Holocene*, *23*(12), 1915–1920. doi: 10.1177/0959683613505336

Prentice, I. C., Harrison, S. P., & Bartlein, P. J. (2011, March). Global vegetation and terrestrial carbon cycle changes after the last ice age. *New Phytologist*, *189*(4), 988–998. doi: 10.1111/j.1469-8137.2010.03620.x

Reis, L. S., Guimarães, J. T. F., Souza-Filho, P. W. M., Sahoo, P. K., de Figueiredo, M. M. J. C., de Souza, E. B., & Giannini, T. C. (2017, August). Environmental and vegetation changes in southeastern Amazonia during the late Pleistocene and Holocene. *Quaternary International*, *449*, 83–105. doi: 10.1016/j.quaint.2017.04.031

Ribas, C. C., Fritz, S. C., & Baker, P. A. (2022, October). The challenges and potential of geogenomics for biogeography and conservation in Amazonia. *Journal of Biogeography*, *49*(10), 1839–1847. doi: 10.1111/jbi.14452

Salati, E., Dall'Olio, A., Matsui, E., & Gat, J. R. (1979). Recycling of water in the Amazon Basin: An isotopic study. *Water Resources Research*, *15*(5), 1250–1258. doi: 10.1029/WR015i005p01250

Scheff, J., & Frierson, D. M. W. (2014). Scaling potential evapotranspiration with greenhouse warming. *Journal of Climate*, *27*(4), 1539–1558. doi: 10.1175/JCLI-D-13-00233.1

Shanahan, T. M., McKay, N. P., Hughen, K. A., Overpeck, J. T., Otto-Bliesner, B., Heil, C. W., ... Peck, J. (2015, February). The time-transgressive termination of the African Humid Period. *Nature Geoscience*, *8*(2), 140–144. doi: 10.1038/ngeo2329

Sherwood, S. C., Ingram, W., Tsushima, Y., Satoh, M., Roberts, M., Vidale, P. L., & O'Gorman, P. A. (2010, May). Relative humidity changes in a warmer climate. *Journal of Geophysical Research*, *115*(D9), D09104. doi: 10.1029/2009JD012585

Shimizu, M. H., Sampaio, G., Venancio, I. M., & Maksic, J. (2020, January). Seasonal changes of the South American monsoon system during the Mid-Holocene in the CMIP5 simulations. *Climate Dynamics*. doi: 10.1007/s00382-020-05137-1

Siler, N., Roe, G. H., Armour, K. C., & Feldl, N. (2019, April). Revisiting the surface-energy-flux perspective on the sensitivity of global precipitation to climate change. *Climate Dynamics*, *52*(7-8), 3983–3995. doi: 10.1007/s00382-018-4359-0

Skonieczny, C., McGee, D., Winckler, G., Bory, A., Bradtmiller, L. I., Kinsley, C. W., … Malaizé, B. (2019, January). Monsoon-driven Saharan dust variability over the past 240,000 years. *Science Advances*, *5*(1), eaav1887. doi: 10.1126/sciadv.aav1887

Staal, A., Tuinenburg, O. A., Bosmans, J. H. C., Holmgren, M., van Nes, E. H., Scheffer, M., … Dekker, S. C. (2018, June). Forest-rainfall cascades buffer against drought across the Amazon. *Nature Climate Change*, *8*(6), 539–543. doi: 10.1038/s41558-018-0177-y

Tapia, P. M., Fritz, S. C., Baker, P. A., Seltzer, G. O., & Dunbar, R. B. (2003, May). A Late Quaternary diatom record of tropical climatic history from Lake Titicaca (Peru and Bolivia). *Palaeogeography, Palaeoclimatology, Palaeoecology*, *194*(1-3), 139–164. doi: 10.1016/S0031-0182(03)00275-X

Tigchelaar, M., & Timmermann, A. (2016, July). Mechanisms rectifying the annual mean response of tropical Atlantic rainfall to precessional forcing. *Climate Dynamics*, *47*(1-2), 271–293. doi: 10.1007/s00382-015-2835-3

van Breukelen, M., Vonhof, H., Hellstrom, J., Wester, W., & Kroon, D. (2008, October). Fossil dripwater in stalagmites reveals Holocene temperature and rainfall variation in Amazonia. *Earth and Planetary Science Letters*, *275*(1-2), 54–60. doi: 10.1016/j.epsl.2008.07.060

van der Ent, R. J. (2016). *WAM-2layers Python.*

van der Ent, R. J., & Savenije, H. H. G. (2013, July). Oceanic sources of continental precipitation and the correlation with sea surface temperature: Precipitation and Correlation with SST. *Water Resources Research*, *49*(7), 3993–4004. doi: 10.1002/wrcr.20296

van der Ent, R. J., Wang-Erlandsson, L., Keys, P. W., & Savenije, H. H. G. (2014, December). Contrasting roles of interception and transpiration in the hydrological cycle – Part 2: Moisture recycling. *Earth System Dynamics*, *5*(2), 471–489. doi: 10.5194/esd-5-471-2014

Venancio, I. M., Mulitza, S., Govin, A., Santos, T. P., Lessa, D. O., Albuquerque, A. L. S., … Schulz, M. (2018, December). Millennial- to Orbital-Scale Responses of Western Equatorial Atlantic Thermocline Depth to Changes in the Trade Wind System Since the Last Interglacial. *Paleoceanography and Paleoclimatology*, *33*(12), 1490–1507. doi: 10.1029/2018PA003437

Vimeux, F., Gallaire, R., Bony, S., Hoffmann, G., & Chiang, J. (2005, December). What are the climate controls on δD in precipitation in the Zongo Valley (Bolivia)? Implications for the Illimani ice core interpretation. *Earth and Planetary Science Letters*, *240*(2), 205–220. doi: 10.1016/j.epsl.2005.09.031

Vuille, M., Bradley, R. S., Werner, M., Healy, R., & Keimig, F. (2003). Modeling δ18O in precipitation over the tropical Americas: 1. Interannual variability and climatic controls. *Journal of Geophysical Research: Atmospheres*, *108*(D6). doi: 10.1029/2001JD002038

Vuille, M., & Werner, M. (2005). Stable isotopes in precipitation recording South American summer monsoon and ENSO variability: Observations and model results. *Climate Dynamics*, *25*(4), 401–413. doi: 10.1007/s00382-005-0049-9

Wang, X., Auler, A. S., Edwards, R. L., Cheng, H., Cristalli, P. S., Smart, P. L., … Shen, C.-C. (2004, December). Wet periods in northeastern Brazil over the past 210 kyr linked to distant climate anomalies. *Nature*, *432*(7018), 740–743. doi: 10.1038/nature03067

Wang, X., Edwards, R. L., Auler, A. S., Cheng, H., Kong, X., Wang, Y., … Chiang, H.-W. (2017, January). Hydroclimate changes across the Amazon lowlands over the past 45,000 years. *Nature*, *541*(7636), 204–207. doi:

10.1038/nature20787

Ward, B. M., Wong, C. I., Novello, V. F., McGee, D., Santos, R. V., Silva, L. C., ... Cheng, H. (2019, April). Reconstruction of Holocene coupling between the South American Monsoon System and local moisture variability from speleothem δ18O and 87Sr/86Sr records. *Quaternary Science Reviews*, *210*, 51–63. doi: 10.1016/j.quascirev.2019.02.019

Whitney, B. S., Mayle, F. E., Punyasena, S. W., Fitzpatrick, K. A., Burn, M. J., Guillen, R., ... Metcalfe, S. E. (2011, July). A 45kyr palaeoclimate record from the lowland interior of tropical South America. *Palaeogeography, Palaeoclimatology, Palaeoecology*, *307*(1-4), 177–192. doi: 10.1016/j.palaeo.2011.05.012

Winnick, M. J., Chamberlain, C. P., Caves, J. K., & Welker, J. M. (2014). Quantifying the isotopic 'continental effect'. *Earth and Planetary Science Letters*, *406*, 123–133. doi: 10.1016/j.epsl.2014.09.005

Worden, Noone, D., Bowman, K., & Tropospheric Emission Spectrometer science team and data. (2007, February). Importance of rain evaporation and continental convection in the tropical water cycle. *Nature*, *445*(7127), 528–532. doi: 10.1038/nature05508

Wortham, B. E., Wong, C. I., Silva, L. C., McGee, D., Montañez, I. P., Troy Rasbury, E., ... Santos, R. V. (2017, April). Assessing response of local moisture conditions in central Brazil to variability in regional monsoon intensity using speleothem 87Sr/86Sr values. *Earth and Planetary Science Letters*, *463*, 310–322. doi: 10.1016/j.epsl.2017.01.034

Wu, H., Guiot, J., Brewer, S., & Guo, Z. (2007, June). Climatic changes in Eurasia and Africa at the last glacial maximum and mid-Holocene: Reconstruction from pollen data using inverse vegetation modelling. *Climate Dynamics*, *29*(2-3), 211–229. doi: 10.1007/s00382-007-0231-3

Zemp, D. C., Schleussner, C.-F., Barbosa, H. M. J., Hirota, M., Montade, V., Sampaio, G., ... Rammig, A. (2017, April). Self-amplified Amazon forest loss due to vegetation-atmosphere feedbacks. *Nature Communications*, *8*(1). doi: 10.1038/ncomms14681

Zular, A., Sawakuchi, A. O., Chiessi, C. M., d'Horta, F. M., Cruz, F. W., Demattê, J. A. M., ... Soares, E. A. A. (2019, January). The role of abrupt climate change in the formation of an open vegetation enclave in northern Amazonia during the late Quaternary. *Global and Planetary Change*, *172*, 140–149. doi: 10.1016/j.gloplacha.2018.09.006